RESEARCH ARTICLE

Computational design and cheminformatics profiling of omeprazole derivatives for enhanced proton pump inhibition of potassium-transporting ATPase alpha chain 1

Mahmudul Hasan[1,2], Md. Ifteker Hossain[1,2], Noimul Hasan Siddiquee[1], Ezaz Ahmed[1,2], Md Walid Hossain Talukder[2,3], Md Rahamatolla[2,4], Tasrin Nahar[2,5], Popy Rani Paul[2,6], Mahmudul Hassan Suhag[7], Monir Uzzaman[2,6]*

1 Faculty of Science, Department of Microbiology, Noakhali Science and Technology University, Noakhali, Bangladesh, 2 Drug Design Division, Computer in Chemistry and Medicine Laboratory, Dhaka, Bangladesh, 3 Faculty of Science, Department of Applied Chemistry and Chemical Engineering, University of Chittagong, Chittagong, Bangladesh, 4 Faculty of Science, Department of Chemistry, University of Rajshahi, Rajshahi, Bangladesh, 5 Department of Chemistry, School of Physical Science, Shahjalal University of Science and Technology, Sylhet, Bangladesh, 6 Faculty of Science, Department of Chemistry, University of Chittagong, Chittagong, Bangladesh, 7 Faculty of Science and Engineering, Department of Chemistry, University of Barishal, Barishal, Bangladesh

* monircu92@gmail.com

Abstract

Proton pump inhibitors are essential for treating moderate-to-severe gastroesophageal reflux, peptic ulcers, esophagitis, and related conditions by increasing gastric pH and inhibiting hydrogen ion discharge into the stomach. However, prolonged use may lead to adverse effects along with reduced efficacy. Our research investigates the strategic modification of omeprazole (OMP) derivatives to improve their binding affinity to targeted proteins, thereby enhancing their chemical reactivity, stability, and toxicity profiles. A total of 22 novel OMP analogues were designed through structural alterations, focusing on the benzimidazole and pyridine rings. The geometrical attributes of the analogues were further confirmed through spectral and quantum computational analysis based on density functional theory (DFT) and a B3LYP/6-31G+ G (d, p) basis set. The molecular docking with PTAAC1 presented that most of the analogues had similar or higher binding affinities and nonbonding interactions, including OMP3, OMP19, and OMP21, with binding energies of -7.3, -8.3, and -8.1 kcal/mol compared to the OMP at -7.1 kcal/mol. Pharmacokinetic, biological, and toxicological profiles via ADMET and PASS predictions also demonstrated increased safety and therapeutic potential. MD simulation also showed good stability of OMP3, OMP19, and OMP21 in binding to PTAAC1, and the RMSD, RMSF, ligand RMSD, rGyr, SASA, MolSA, PolSA, and hydrogen bond analysis also suggested superior drug potential compared to OMP. Additionally, the post-simulation MM/GBSA analysis revealed that OMP3 (-36.91 kcal/mol) outperformed OMP19 (-26.45) and OMP21

(-12.61). The protein binding site's high stability and elevated negative binding free energy value further indicate a robust compound-protein interaction with OMP3. However, principal component analysis (PCA) showed the highest variance for OMP21, accounting for 50.66%, 21.58%, and 6.51%, respectively, for PC1, PC2, and PC3. These findings could lead to the development of OMP3 and OMP21 as potential next-generation PPIs with enhanced pharmacological activity and improved side-effect profiles, necessitating more *in vitro* and *in vivo* testing.

1 Introduction

Proton pump inhibitors (PPIs) are essential medications recognized by the World Health Organization (WHO), used as a cornerstone of drug therapy for patients with moderate-to-severe Gastroesophageal Reflux Disease (GERD) symptoms and esophagitis [1,2]. PPIs increase gastric pH by covalently binding to the H^+/K^+-ATPase antiporter pumps of the gastric parietal cells, inhibiting hydrogen ion discharge into the stomach [3]. PPIs are superior to traditional treatment options like sucralfate, antacids, and histamine-2 receptor antagonists (H_2RAs) due to their high effectiveness and rapid increase in gastric pH [4–6]. They have recently replaced H_2RAs in treating many acid-related conditions, as they are not associated with the rapid tachyphylaxis seen with H_2RAs, the most widely used agents in prophylactic acid suppression [4].

There are currently six Food and Drug Administration (FDA)-approved PPIs: rabeprazole, lansoprazole, pantoprazole, esomeprazole, omeprazole, and dexlansoprazole. These PPIs can effectively treat and prevent conditions like acid reflux, peptic ulcer disease, and first-line treatment for *Helicobacter*-induced gastrointestinal lesions [7], duodenal ulcers, and Zollinger-Ellison syndrome [8,9]. These were sequentially developed due to varying pharmacokinetic parameters, such as extended plasma half-life, routes of administration, and drug interactions [10,11]. Pantoprazole and rabeprazole, used in recommended dosages, maintain esophageal healing and provide symptom relief similar to omeprazole and lansoprazole [12].

In general, the stomach's acids play a significant role in the digestion of nutrients; however, lowering these acids can help with indigestion and heartburn. The stomach produces acidic liquids with a pH value of about 1.5 to 3.5, which kills microorganisms and facilitates the digestion and absorption of nutrients like protein, iron, calcium, and vitamin B12 [13]. However, as this produced acid may harm the digestive system, several protective mechanisms, such as mucosal mucous, bicarbonate barrier, and gastroesophageal junction sphincter contraction, are present to guard against injury to the gastroesophageal junction brought on by gastric secretion [14,15]. When acid secretion overcomes such protective processes, the gastrointestinal mucosa might become injured and inflamed, resulting in unpleasant symptoms or pathological illness [15]. These pathological illnesses, including Barrett's esophagus, gastroduodenal ulcers, GERD, and functional dyspepsia, are known as acid-related diseases [16,17]. After beginning to be used clinically for the treatment of disorders

associated with acid reflux, the usage of PPIs developed consistently and significantly, and now they are among the most often prescribed medications worldwide [18].

Like any other clinical medication, PPIs also come with their own set of benefits and side effects. Compared to H_2RAs, long-term use of PPIs is associated with a slightly higher risk of certain side effects [19]. Prolonged use is accumulating evidence of adverse side effects, yet the causal relationship between these symptoms remains unclear. These include a higher chance of getting community-acquired pneumonia, an enteric infection, gastrointestinal tract cancer, malabsorption of many nutrients, vitamins, and minerals, having a myocardial infarction, breaking bones (most often in the hip, spine, and wrist), diarrhoea, a *Clostridium difficile* infection, a stroke, Alzheimer's dementia, and kidney damage [18,20–29]. For patients with fewer side effects, creating a PPI with a longer half-life that will block stomach proton pumps for a more extended period and possibly have a more significant acid suppression effect is crucial. It is important to note that several research teams have been developing potassium-competitive acid blockers and PPIs to investigate longer-lasting and more potent acid inhibition [30–32].

Structural modification of existing drugs can improve their pharmacological properties, potentially leading to more effective and improved therapeutics by rationally altering their molecular structure [33–35]. Such changes can influence drug behaviour by affecting its electrical distribution, polarity, hydrogen bonding capacity, and steric profiles. These alterations influence target binding, solubility, metabolic stability, and bioavailability by altering the molecular composition, weight, and substituent position. This rational design approach enables the development of drug candidates with improved target selectivity, fewer side effects, and the advancement of therapeutic efficacy and safety. This study seeks to develop novel therapeutic alternatives to improve the therapeutic efficacy, potency, and side effects of OMP. Omeprazole was structurally modified and computationally studied by substituting functional groups like $-OCH_3$, $-CF_3$, $-OCF_3$, $-NH_2$, $-CH_2NH_2$, $-NHCONH_2$, and $-NHCOCH_3$ for the methoxy groups in the benzimidazole and pyridine rings and the alkyl group in the pyridine ring, resulting in 22 derivatives in this study. The electron-donating or withdrawing effect of functional groups has an impact on the dipole moment, free energy, and the band gap values between the highest occupied molecular orbitals (HOMO) and the lowest unoccupied molecular orbitals (LUMO). The strong electron-withdrawing nature of fluorine leads to an increase in dipole moment in the presence of electronegative atoms or polar bonds [36]. The trifluoromethoxy ($-OCF_3$) group exhibits the largest dipole moment, followed by the acetamido group ($-NHCOCH_3$), which contains a polar carbonyl and an amide group. Through the donation of their lone pairs and the influence of resonance, the methoxy ($-OCH_3$) and amino ($-NH_2$) groups contribute to an increase in the dipole moment. Regarding free energy, electron-donating groups ($-OCH_3$, $-NH_2$) contribute to the stabilization of the molecule, leading to a decrease in free energy; in contrast, electron-withdrawing groups ($-OCF_3$, $-NHCOCH_2$) result in the destabilization of the molecule, thereby increasing free energy [37]. About the HOMO-LUMO gap, the presence of electron-donating groups pushes electro into the system, therefore raising the HOMO level, decreasing the gap, and increasing molecular reactivity, while electron-withdrawing groups increase the gap by pulling electrons from the system, stabilizing the molecule and reducing its reactivity [38]. The presence of the $-OCF3$ and $-NHCOCH3$ groups led to an expansion of the HOMO-LUMO gap, thereby enhancing stability. In contrast, the $-OCH_3$ and $-NH_2$ groups contribute to an overall increase in reactivity. These computational chemistry-based modifications of the drug can maximize the pharmacological efficacy, stability, and bioactivity, supporting the development of novel drugs with increased efficacy and reduced side effects. However, more research is necessary to validate and identify a superior drug alternative.

This study provides a detailed *in-silico* analysis of the reference compound OMP and twenty-two of its structural analogues. It evaluates the thermodynamic properties, frontier molecular orbitals, electrostatic potential maps, Fourier transform infrared spectroscopy (FT-IR), and UV–Visible spectral profiles. Furthermore, molecular docking, non-bonding interactions, ADMET characteristics, and PASS predictions were explored. Following these findings, selected analogues were subjected to molecular dynamics simulations to assess their stability and binding behaviour over time. This study

appears to be the first comprehensive computational investigation providing insights into physicochemical, spectral, and biological characteristics while aiding in the rational design of effective, safer therapeutic candidates.

2 Methodology and computational details

2.1 Geometry optimization

Quantum mechanical methods have significantly aided computational drug design by predicting molecular orbitals, electrostatic potential, and thermodynamic properties [39,40]. The initial geometry of OMP was obtained from the PubChem online database (PubChem CID: 4594). The Gabedit (version 2.5.0) software was used to determine the compounds' most stable and lowest-energy conformation. The structural modification and geometry optimization of all compounds was conducted using the Gaussian 09 W Revision D.01 package, employing CAM-B3LYP and DFT at the 6-31G+ (d, p) level of theory [41,42]. The electronic transitions of the compounds were also determined using the time-dependent density functional theory (TD-DFT) with the same basis set [43]. All the compounds presented in Tables 1, S1 and S1 Fig in S1 File have been analyzed for a range of properties, such as enthalpy, free energy, electrostatic potential, dipole moment, and vibrational frequencies. Frontier molecular orbital features HOMO, and LUMO were calculated at the same theoretical level as follows [44].

$$\text{Gap } (\Delta E) = [\varepsilon \text{LUMO} - \varepsilon \text{HOMO}] \tag{1}$$

Table 1. Molecular formula (MF), molecular weight (MW) of OMP, and its newly designed analogues (the remaining ones are presented in S1 and S2 Tables in S1 File).

Name	R_1	R_2	R_3	MF	MW (g/mol)
OMP	CH_3	OCH_3	OCH_3	$C_{17}H_{19}N_3O_3S$	345.416
OMP1	OCH_3	OCH_3	OCH_3	$C_{17}H_{19}N_3O_4S$	361.415
OMP2	CF_3	OCH_3	OCH_3	$C_{17}H_{16}F_3N_3O_3S$	399.387
OMP3	CH_3	CF_3	OCH_3	$C_{17}H_{16}F_3N_3O_2S$	383.388
OMP4	CH_3	OCH_3	CF_3	$C_{17}H_{16}F_3N_3O_2S$	383.388
OMP5	OCF_3	OCH_3	OCH_3	$C_{17}H_{16}F_3N_3O_4S$	415.387
OMP6	CH_3	OCF_3	OCH_3	$C_{17}H_{16}F_3N_3O_3S$	399.387
OMP7	CH_3	OCH_3	OCF_3	$C_{17}H_{16}F_3N_3O_3S$	399.387
OMP8	NH_2	OCH_3	OCH_3	$C_{16}H_{18}N_4O_3S$	346.404
OMP9	CH_3	NH_2	OCH_3	$C_{16}H_{18}N_4O_2S$	330.405
OMP10	CH_3	OCH_3	NH_2	$C_{16}H_{18}N_4O_2S$	330.405
OMP11	CH_2NH_2	OCH_3	OCH_3	$C_{17}H_{20}N_4O_3S$	360.431
OMP12	CH_3	CH_2NH_2	OCH_3	$C_{17}H_{20}N_4O_2S$	344.431
OMP13	CH_3	OCH_3	CH_2NH_2	$C_{17}H_{20}N_4O_2S$	344.431
OMP14	$CONH_2$	OCH_3	OCH_3	$C_{17}H_{18}N_4O_4S$	374.414
OMP15	CH_3	$CONH_2$	OCH_3	$C_{17}H_{18}N_4O_3S$	358.415
OMP16	CH_3	OCH_3	$CONH_2$	$C_{17}H_{18}N_4O_3S$	358.415
OMP17	$NHCONH_2$	OCH_3	OCH_3	$C_{17}H_{19}N_5O_4S$	389.429
OMP18	CH_3	$NHCONH_2$	OCH_3	$C_{17}H_{19}N_5O_3S$	373.429
OMP19	CH_3	OCH_3	$NHCONH_2$	$C_{17}H_{19}N_5O_3S$	373.429
OMP20	$NHCOCH_3$	OCH_3	OCH_3	$C_{18}H_{20}N_4O_4S$	388.440
OMP21	CH_3	$NHCOCH_3$	OCH_3	$C_{18}H_{20}N_4O_3S$	372.441
OMP22	CH_3	OCH_3	$NHCOCH_3$	$C_{18}H_{20}N_4O_3S$	372.441

https://doi.org/10.1371/journal.pone.0326655.t001

$$\eta = \frac{[\varepsilon\text{LUMO} - \varepsilon\text{HOMO}]}{2} \tag{2}$$

$$S = \frac{1}{2\eta} \tag{3}$$

$$\mu = \frac{[\varepsilon\text{LUMO} + \varepsilon\text{HOMO}]}{2} \tag{4}$$

$$\chi = -\frac{[\varepsilon\text{LUMO} + \varepsilon\text{HOMO}]}{2} \tag{5}$$

$$\omega = \frac{\mu^2}{2\eta} \tag{6}$$

were applied for calculating the HOMO-LUMO gap, hardness (η), softness (S), chemical potential (μ), electronegativity (χ), and electrophilicity (ω).

2.2 Protein preparation, molecular docking, and interactions

Molecular docking is crucial in drug discovery and computational biology, predicting drug interactions with proteins or binding sites using various algorithms and methodologies developed over the years [45,46]. The target protein for proton pump inhibitors was initially identified as potassium-transporting ATPase alpha chain 1 (PTAAC1) with a molecular weight of 114117.74 Da and Uniprot ID P20648. The protein was predicted using AlphaFold and has a very high model confidence value (pLDDT > 90), which employs novel neural network topologies and training approaches based on geometric, physical, and evolutionary constraints to improve structure prediction accuracy [47]. The protein was a transmembrane protein and a human ATP4A gene product. The 3D crystal structure of PTAAC1 was then obtained using the AlphaFold Protein Structure Database. The protein structure underwent energy minimization using Swiss-PdbViewer (Version 4.1.0) software to reduce weak interatomic interactions within the protein [48]. The PyRx (Version 0.8) software package was used for molecular docking against the energy-minimized PTAAC1 protein, analyzing proteins as macromolecules and optimizing OMP and its analogues as ligands [49]. Docking was carried out after the ligands and proteins were loaded. The software command was used to set the box size to the highest dimension level, with a center grid box size of 112.59 Å, 83.32 Å, and 108.49 Å in the x, y, and z-axis directions, respectively. This enabled the grid box to encase the protein structure entirely. The visual examination of the active site was conducted with BIOVIA Discovery Studio Visualizer 2021. Further, the study utilized molecular docking and nonbonding interaction computations to assess ligands' stability and binding effectiveness within protein binding sites, analyzing docking findings and providing cumulative results. After evaluating different parameters, the selected compounds for simulation were further re-docked and visualized using Maestro v13.5 for docking validation.

2.3 ADMET and PASS prediction

Pharmaco-informatics is a vital part of designing novel drugs. During preclinical drug development, it is important to evaluate a drug's chemical absorption, distribution, metabolism, excretion, and toxicity. To predict these properties, the AdmetSAR online server (http://lmmd.ecust.edu.cn/admetsar2/) was utilized [50]. In addition, to forecast biological activity profiles and identify drug-like organic compounds based on their structural formulas, the PASS (Prediction of Activity Spectra for Substances) web server (http://www.way2drug.com/passonline/) was employed [51]. Both evaluations were conducted using SMILES (Simplified Molecular Input Line Entry System) and structural data files to generate the results.

2.4 Molecular dynamics simulation analysis

Molecular dynamics (MD) simulation was used to investigate the protein-ligand complex's structural stability under a specific physiological setting. To confirm the stability of the protein-ligand complex, 100 ns MD simulations were used to examine the selected compound's (OMP3, OMP19, OMP21, and OMP as a control) ability to bind the targeted PTAAC1 protein. The Schrödinger suite's Desmond Maestro v13.5 was used to run an MD simulation for 100 ns. The protein preparation wizard was used to pre-process the complex structure after molecular docking investigations of protein-ligand complexes. An orthorhombic periodic boundary box shape with an interval of 10 × 10 × 10 Å^3 was employed for each complex simple point-charge (SPC) water model that was utilized to analyze the system to preserve its volume. The solvated system was randomly supplemented with Na$^+$ and Cl$^-$ ions to keep the salt concentration at 0.15 M. Through the use of the OPLS4 force field, the system was relaxed and mitigated. Lastly, the constant pressure-constant temperature (NPT) ensemble was implemented at 1.01325 bar of pressure and 300.0 K of temperature. After the system had been relaxed for each complex, the final production cycle was executed with an energy of 1.2 and 100 ps recording intervals.

3 Results and discussion

3.1 Thermodynamics analysis

Thermodynamic analysis, such as Gibbs free energy, enthalpy, and dipole moment, is crucial for comprehending the stability of drug-receptor interactions, molecular behaviour, and binding efficiency [52]. Subtle structural modifications of a compound can significantly impact the thermodynamic properties, influencing the overall pharmacokinetic profile [53,54]. The negative value of free energy can predict the chemical stability, binding affinity, and spontaneity of a reaction, an important criterion for reflecting binding partners' interactions [55,56]. As shown in **Fig 1**, OMP has a free energy of -1447.092 Hartree. In comparison, OMP5 exhibits the largest negative value (-1820.005 Hartree) due to replacing the –CH$_3$ functional group with the –OCF$_3$ functional group in the R$_1$ position of the core structure. The –OCF$_3$ group exhibits a significant electron-withdrawing potential, stabilizes the molecule's electronic structure, and lowers its energy relative to the electron-donating –CH$_3$ group. Regarding free energy, all OMP analogues exhibit larger negative free energy values compared to OMP, except OMP9, OMP10, OMP12, and OMP13, which separately replace the –OCH$_3$ functional group in the R$_2$ and R$_3$ positions with the –NH$_2$ group and the –CH$_2$NH$_2$ group. Substituting –OCH$_3$ with –NH$_2$ and –CH$_2$NH$_2$ results in more pronounced electron-donating effects and possible hydrogen-bonding interactions. These changes may stabilize positive charges, improve solubility, or influence reactivity at the R$_2$ and R$_3$ positions, contingent upon the molecular context. The significant negative free energy values of all analogous compounds indicate that these are more stable in terms of energy and configuration. The polarity of a molecule can be determined by measuring the dipole moment. The compounds' polar characteristics and dipole moments contribute to the binding affinity and nonbonding interactions between drugs and receptor proteins in complexes [57,58]. The dipole moment values are influenced by the functional group and its position within analogues. The analysis revealed that OMP17 exhibited the lowest dipole moment values, while OMP18 showed the highest (Fig 1b, S3 Fig in S1 File). The dipole moment of OMP is measured at 4.398 Debye; in contrast, most of its analogues exhibit higher dipole moment values. These analogues' elevated dipole moment values suggest greater binding affinity, hydrogen bonding, and nonbonding interaction capabilities than OMP. Alongside, the highest electrophilicity was observed for OMP2 (3.074 eV), correlating with enhanced reactivity but posing a risk of kinetic instability owing to its low thermodynamic stability. OMP19 and OMP21 emerged as balanced candidates, combining moderate stability and reactivity. Conversely, OMP7, OMP10, OMP18, and OMP22 showed limited drug-likeness owing to excessive polarity (dipole >10) or positive internal energy, whilst OMP8 and OMP9 were deemed unsuitable due to elevated internal energy and reduced stability. All the thermodynamic results, summarized in Fig 1, Tables 1, and 2, highlight critical stability-solubility trade-offs for drug development.

3.2 Frontier molecular orbital analysis

The energy gaps between the HOMO and LUMO exhibited by the OMP analogues serve as important indicators of their tendency for electron transfer. This property influences the compound's reactivity, stability, chemical softness, hardness, electrophilicity, and chemical potential values. Therefore, it plays a significant role in the broader context of our research. The control OMP demonstrates a moderate gap, serving as a baseline for assessing the reactivity and stability of the other analogues. The differences observed in HOMO-LUMO gaps across the analogues highlight the influence of
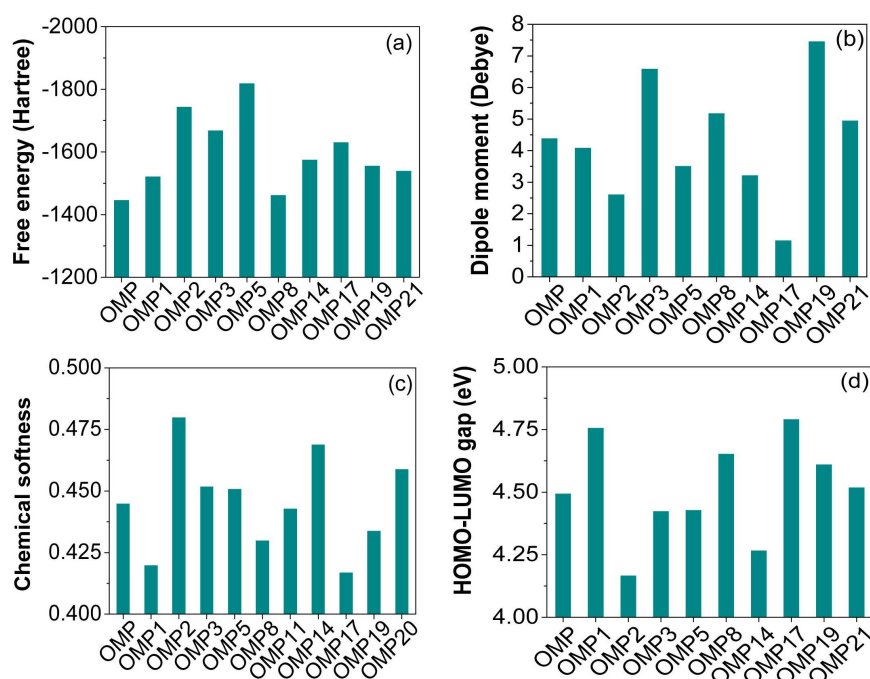
Fig 1. Free energies (Hartree) (a), dipole moments (Debye) (b), chemical softness (c), and HOMO-LUMO gaps (d) of OMP and a few selected analogues (remaining values are presented in S3 Fig in S1 File).

https://doi.org/10.1371/journal.pone.0326655.g001

Table 2. Energy (eV) of HOMO, LUMO, hardness (η), chemical potential (μ), electronegativity (χ), and electrophilicity (ω) of OMP and its analogues (remaining are presented in S2 Table in S1 File).

Name	ϵHOMO	ϵLUMO	η	μ	χ	ω
OMP	-5.836	-1.342	2.247	-3.589	3.589	2.866
OMP1	-5.855	-1.097	2.379	-3.476	3.476	2.539
OMP2	-5.663	-1.495	2.084	-3.579	3.579	3.074
OMP3	-5.742	-1.317	2.213	-3.530	3.530	2.815
OMP5	-5.563	-1.133	2.215	-3.348	3.348	2.531
OMP8	-5.427	-0.773	2.327	-3.100	3.100	2.065
OMP11	-5.542	-1.029	2.257	-3.285	3.285	2.391
OMP14	-5.619	-1.351	2.134	-3.485	3.485	2.846
OMP17	-5.756	-0.963	2.396	-3.360	3.360	2.355
OMP19	-5.551	-0.940	2.306	-3.246	3.246	2.284
OMP20	-5.431	-1.073	2.179	-3.252	3.252	2.426
OMP21	-5.554	-1.034	2.260	-3.294	3.294	2.401

https://doi.org/10.1371/journal.pone.0326655.t002

different substituents on electronic behaviour. Notably, OMP4 exhibits the highest energy gap of 5.020 eV, suggesting higher energy is required for its excitation. Incorporating a strong electron-withdrawing group like –CF$_3$ into the molecular structure might facilitate the tight binding of electrons while simultaneously reducing their delocalization. This alteration is likely to enhance the overall stability of the compound OMP4 while concurrently reducing its reactivity. In contrast, OMP2 demonstrated the smallest gap of 4.168 eV, underscoring the notable influence of electron-withdrawing groups like –OCH$_3$ in its composition. This, in turn, results in high electrophilic reactivity but potential instability. The nuanced variations in energy gaps among the OMP derivatives, including OMP1, OMP21, OMP11, and others. Compared to OMP, OMP3 exhibits a smaller gap of 4.425 eV, suggesting a likely increase in electronic reactivity due to a possible electron donor effect. Conversely, OMP19 exhibits a larger gap of 4.612 eV compared to the control, indicating enhanced stability and reduced reactivity. OMP21 exhibited a difference of 4.520 eV from the control, suggesting minimal electronic alteration. Among the remaining analogues, the gap values, ranging from 4.300 to 4.800 eV, prove the varying effects and balance substitution of electron-donating and withdrawing group effects, which tune orbital energies. Table 2, Figs 1c and 2 depict the molecular orbitals (HOMO and LUMO) and the HOMO-LUMO energy gap, respectively, of the OMP and a few selected analogues.

3.3 Molecular electrostatic potential analysis

Molecular Electrostatic Potential (MEP) map provides a visual representation of charge distribution within a compound, aiding in predicting a drug's reactivity, binding regions, and sites [59]. It is crucial in computational chemistry to identify the probable sites for electrophilic or nucleophilic attack to understand a chemical reaction [60]. This highlights the negatively charged electron-rich region (red colour), and the electron-deficient region, positively charged region (blue colour), allowing the identification of potential sites for hydrogen bonding, ionic interactions, and other noncovalent forces [61,62].

εLUMO= -1.097 eV   εLUMO= -0.999 eV   εLUMO= -1.332 eV

Gap = 4.758 eV   Gap = 4.826 eV   Gap = 5.020 eV

εHOMO= -5.855 eV   εHOMO= -5.825 eV   εHOMO= -6.352 eV

OMP   OMP13   OMP4
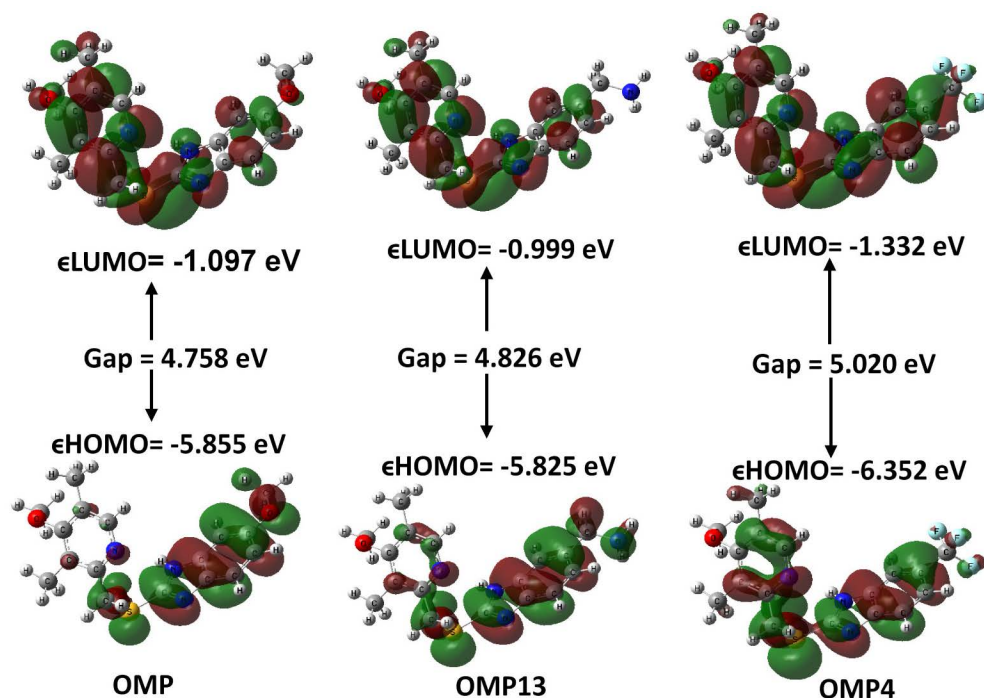
Fig 2. Molecular orbitals (HOMO and LUMO) and HOMO-LUMO energy gap of OMP and a few selected analogues (remaining values are presented in S2 Fig in S1 File).

https://doi.org/10.1371/journal.pone.0326655.g002

MEP maps facilitate structure-activity relationship studies and binding efficacy by providing comprehensive insights into the electrostatic complementarity between the ligand and its target [59,63]. Our analysis reveals that OMP possesses moderate electrostatic potential values, suggesting a balanced reactivity with electrophilic and nucleophilic tendencies (-0.2339 Hartree and +0.1809 Hartree). Compared to the control, OMP9 and OMP18 exhibit the highest negative potentials of -0.3215 Hartree and -0.3164 Hartree, respectively. This suggests a strong electrophilic characteristic, which could enhance their reactivity toward nucleophilic biological sites. Conversely, OMP3 exhibits the highest positive potential at +0.2740 Hartree, suggesting a pronounced nucleophilic nature, likely favoring interactions with electrophilic targets (Fig 3). Other analogs, such as OMP5 and OMP10, displayed moderate potentials, suggesting well-balanced reactivity profiles that position them as promising candidates for drug development, as they integrate stability with selective reactivity. Overall, the moderate electrostatic potentials of many analogs suggest they offer a promising balance of reactivity for therapeutic applications. At the same time, the variations observed in OMP9, OMP18, and OMP3 simultaneously present opportunities for focusing on more precise interactions.

3.4 Vibrational frequencies (FT-IR) analysis

FT-IR spectral analysis is an essential technique for inspecting the chemical structure of any compound, effectively confirming the existence of various functional groups within the molecule. In our study, the FT-IR spectral vibrational frequencies are calculated in the 400-4000 cm^{-1} range to prove the existence of intended functional groups for OMP and its analogues (Fig 4). The data were then adjusted by multiplying a scaling factor 0.9688 to improve accuracy, as shown in S3 Table in S1 File. The peaks observed at 976-1071 cm^{-1} attributed to the stretching of the S=O groups confirm the presence of S=O groups in all compounds. All optimized compounds exhibit stretching frequency bands ranging from 3495 to 3575 cm^{-1} for the N-H bond present in the imidazole units of their structure. Additionally, the stretching frequency was detected within the ranges of 1571-1627 cm^{-1}, 3039-3147 cm^{-1}, and 2895-2935 cm^{-1}, indicating the presence of C=N, aromatic C-H, and aliphatic C-H bonds in all compounds. The N-H vibrations in groups, such as –NH$_2$, –CH$_2$NH$_2$, –CONH$_2$, –NHCONH$_2$, and –NHCOCH$_3$, are observed in the OMP analogues within the 3425-3501 cm^{-1} range. Furthermore, some analogues have observed at the spectral bands at 1717-1745 cm^{-1} correspond to the carbonyl group (C=O) present in –CONH$_2$, –NHCONH$_2$, and –NHCOCH$_3$, which are incorporated through modifications. The variation in the stretching frequency position for each was observed concerning the structural modification of the OMP at different positions using different functional groups.
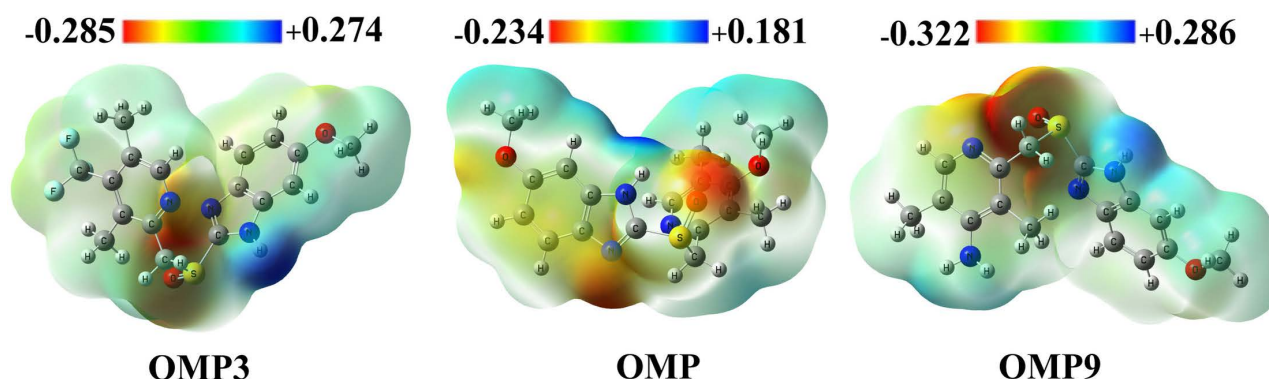
Fig 3. Electrostatic potential map of OMP, OMP9, and OMP18 (remaining values are presented in S4 Fig in S1 File).

https://doi.org/10.1371/journal.pone.0326655.g003

3.5 UV-visible spectral analysis

UV-visible spectroscopy is essential in developing novel drug compounds, offering insights into molecular properties and interactions. This method is crucial for identifying functional groups that influence a drug's biological activity by analyzing the electronic transitions in molecules and revealing information about conjugated systems, aromatic rings, or chromophores [64]. Our analysis focused on assessing the synthesized OMP analogues' absorption properties and drawing comparisons with the OMP to pinpoint modifications that could improve therapeutic efficacy. Pronounced red shifts in $S_0 \rightarrow S_1$ transitions were observed for analogues, like OMP3 ($\lambda_{max} = 953.120$ nm) and OMP19 ($\lambda_{max} = 1130.760$ nm), attributed to extended π-conjugation, that can be strategically enhanced through the addition of functional groups. Electron-donating groups (e.g., $-OCH_3$, $-NH_2$) and electron-withdrawing groups (e.g., $-OCF_3$, $-NHCOCH_2$) influence the electron density across π-system, accelerate the intramolecular charge transfer, and improve the delocalization. Such substituents improve conjugation and reduce the HOMO–LUMO gap when positioned effectively, leading to a significant red shift. These structural modifications influence the electronic stability, membrane permeability, and binding affinity towards the target, which are crucial for the rational design of different, more potent candidates for drug development. OMP21 was identified as red shift absorption ($\lambda_{max} = 762.640$ nm), suggesting the enhanced π-conjugation and moderate excitation probability, making it a potential candidate for increased membrane permeability and prolonged biological activity with H^+/K^+-ATPase protein. OMP8 ($\lambda_{max} = 695.100$ nm) and OMP12 ($\lambda_{max} = 678.890$ nm) possess absorption values close to OMP ($\lambda_{max} = 680.250$ nm), indicating their structural similarities and balanced modifications, while slight red shift suggests improved pharmacokinetic properties. Additionally, weak transition probabilities were noted for OMP14, OMP15, OMP18, and OMP22 despite having red shift λ_{max} values, suggesting limited electronic excitation. This indicates that further modifications are required to improve these analogues for better conjugation, charge transfer, and overall pharmacokinetic and pharmacodynamic properties. Absorption characteristics, such as the maximum wavelengths, excitation energies, and oscillator strengths for each molecule, were compiled in S4 Table in S1 File. Additionally, Fig 5 visualized the UV-Vis spectra of these molecules.

3.6 Binding affinity and interactions analysis

Molecular docking is a crucial computational technique in drug design that optimizes the spatial arrangement of ligands and proteins to anticipate interaction strength, akin to a lock and key mechanism [45,46]. It also contributes to accurate hit detection, lead optimization, and rational drug design, making it a promising option for future drug discovery. The clinical understanding of the binding affinities of the synthesized OMP analogues improved through a comparative analysis of
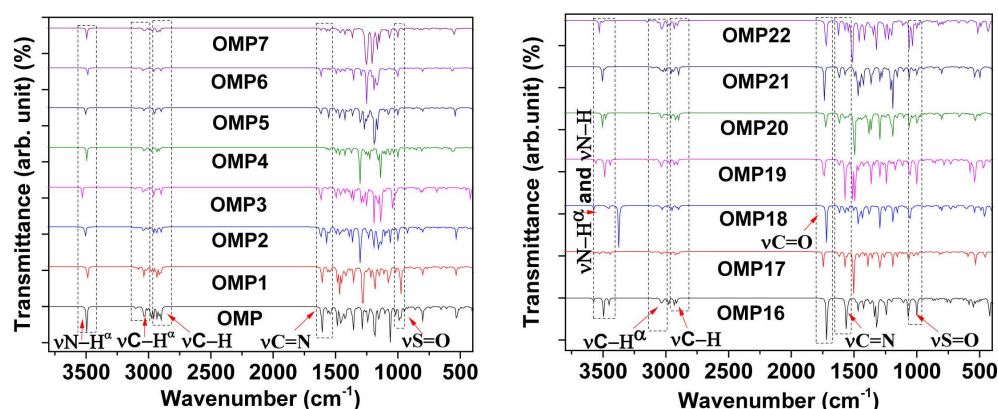
Fig 4. FT-IR spectra of OMP and its analogues (remaining values are presented in S5 Fig in S1 File).

https://doi.org/10.1371/journal.pone.0326655.g004

their binding energies to those of widely recognized commercial proton pump inhibitors (PPIs), such as pantoprazole, esomeprazole, and omeprazole (control). The calculated binding energies for pantoprazole, esomeprazole, and omeprazole were -7.2 kcal/mol, -7.3 kcal/mol, and -7.0 kcal/mol, respectively, in association with the targeted PTAAC1 protein. An increased binding affinity of several OMP analogues was observed, with binding energies ranging from -6.9 kcal/mol to -8.3 kcal/mol (S7 and S8 Figs, S5 Table in S1 File). In particular, OMP (-7.0 kcal/mol), OMP3 (-7.9 kcal/mol), OMP4 (-7.7 kcal/mol), OMP6 (-7.5 kcal/mol), OMP17 (-7.8 kcal/mol), OMP18 (-7.6 kcal/mol), OMP19 (-8.3 kcal/mol), and OMP21 (-8.1 kcal/mol) exhibited enhanced binding interactions compared to both the control (OMP) and established PPIs. The findings also reveal the presence of multiple binding pockets for analogues and highlight a variety of nonbonding interactions such as alkyl, hydrogen, carbon-hydrogen, conventional hydrogen, hydrophobic bonds, and others which are critical for drug stability and binding affinity in the ligand-protein complex. By changing binding preferences and making preferred ligands more stable, hydrogen and hydrophobic bonds improve the effectiveness of drugs. Strong hydrogen bonding with less than 2.3 Å increases binding affinity, while excellent bond distances are observed in most analogues [39]. The enhanced binding affinities observed in the OMP analogues can be attributed to their distinct molecular interactions with specific amino acid residues located within the binding pocket of the relevant target protein. The non-bonding interactions of OMP (control) were identified to form hydrogen bonds with ASN991 (2.402 Å), TYR801 (2.965 Å), and ASP139 (2.535 Å) as shown in Table 3 and Fig 6. Among the analogues, OMP3 (-7.9 kcal/mol) demonstrated notable interactions with key residues, such as LYS784 (H bond, 2.039 Å), ARG951 (H bond, 2.279 Å), and ASP853 (H bond, 2.687 Å). Moreover, OMP3 interacted with hydrophobic residues like ARG777 and ILE842, stabilizing the binding complex. A comparable trend was noted with OMP19 (−8.3 kcal/mol), which established multiple interactions, carbon-hydrogen bonds with SER380 (2.572 Å), and hydrophobic interactions with LEU378 (2.508 Å) and ILE722 (2.255 Å), thus improving its binding affinity. OMP21 exhibited a binding energy of -8.1 kcal/mol, showcasing notable interactions, including a hydrogen bond with THR381 (2.711 Å), carbon-hydrogen bond with ASP740 (2.103 Å) and GLU376 (2.254 Å), contributed significantly to its binding. The findings suggest that the OMP analogues, especially OMP3, OMP19 and OMP21, exhibit enhanced binding affinities compared to commercially available PPIs, hence selected for further studies. This molecular docking underscores the complex web of nonbonding interactions in the ligand-protein complex (OMP and its analogues with PTAAC1), highlighting their potential contribution to enhanced pharmacological effects, including improved potency and selectivity.
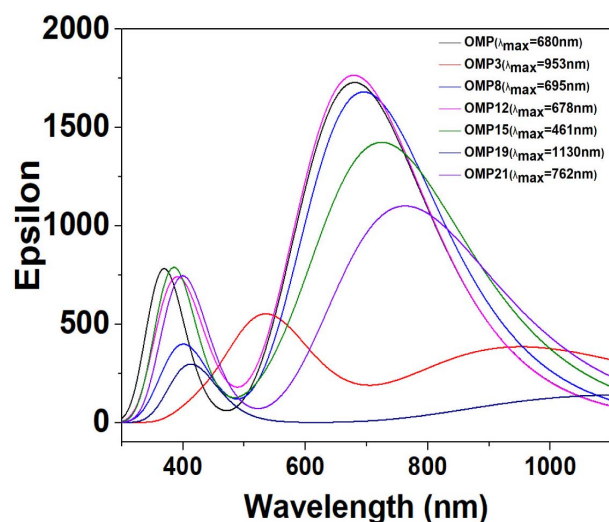
Fig 5. UV-visible spectra of OMP and a few of its analogues (remaining values are presented in S6 Fig in S1 File).

https://doi.org/10.1371/journal.pone.0326655.g005

Table 3. Binding affinity and nonbonding interactions of lead and control compounds with the PTAAC1 protein.

Name	Binding affinity (kcal/ mol)	Residues in contact	Interaction type	Distance (Å)
OMP	-7	ASN991	H	2.40238
		TYR801	H	2.96557
		ASP139	H	2.53565
		ALA337	A	4.01548
		VAL333	A	4.77205
		LEU923	A	5.33114
		TYR801	PA	5.31099
		PHE919	PA	4.84499
OMP3	-7.9	LYS784	H	2.03935
		ARG951	H	2.27993
		ASP853	H	2.68796
		ARG777	X	3.05064
		TYR1034	PSu	5.89964
		ARG848	A	3.45658
		ARG777	A	4.11721
		ARG848	A	4.30438
		ARG777	A	3.89063
		ILE842	A	4.49137
		LEU845	A	5.08436
		PHE780	PA	4.41439
		PHE780	PA	4.888
OMP19	-8.3	LEU378	C	2.50852
		SER380	C	2.57251
		ILE722	C	2.25577
		ILE722	C	2.1259
		ILE722	PS	3.60635
		ILE722	A	3.70575
		PRO294	PA	5.27908
		LEU378	PA	4.55256
		ILE741	PA	5.26048
OMP21	-8.1	THR381	H	2.71146
		ASP740	C	2.1039
		GLU376	C	2.25455
		ALA374	A	3.63098
		LEU378	A	5.36355
		LEU378	A	4.52511
		ILE722	A	4.60832
		VAL773	A	3.95789
		PRO294	PA	4.515
		ALA724	PA	4.34429

Here, A = Alkyl, APS = Amide-pi stacked, C = Carbon hydrogen Bond, H = Conventional hydrogen bond, HB = Hydrogen bond, HP = Hydrophobic bond, PA = Pi-alkyl, Pa = Pi-anion, PC = Pi-cation, Pd = Pi-donor, PS = Pi-sigma, PSu = Pi-sulfur, PPS = Pi-Pi stacked, PPTSh = Pi-Pi T-shaped, X = Halogen (Fluorine) bond.
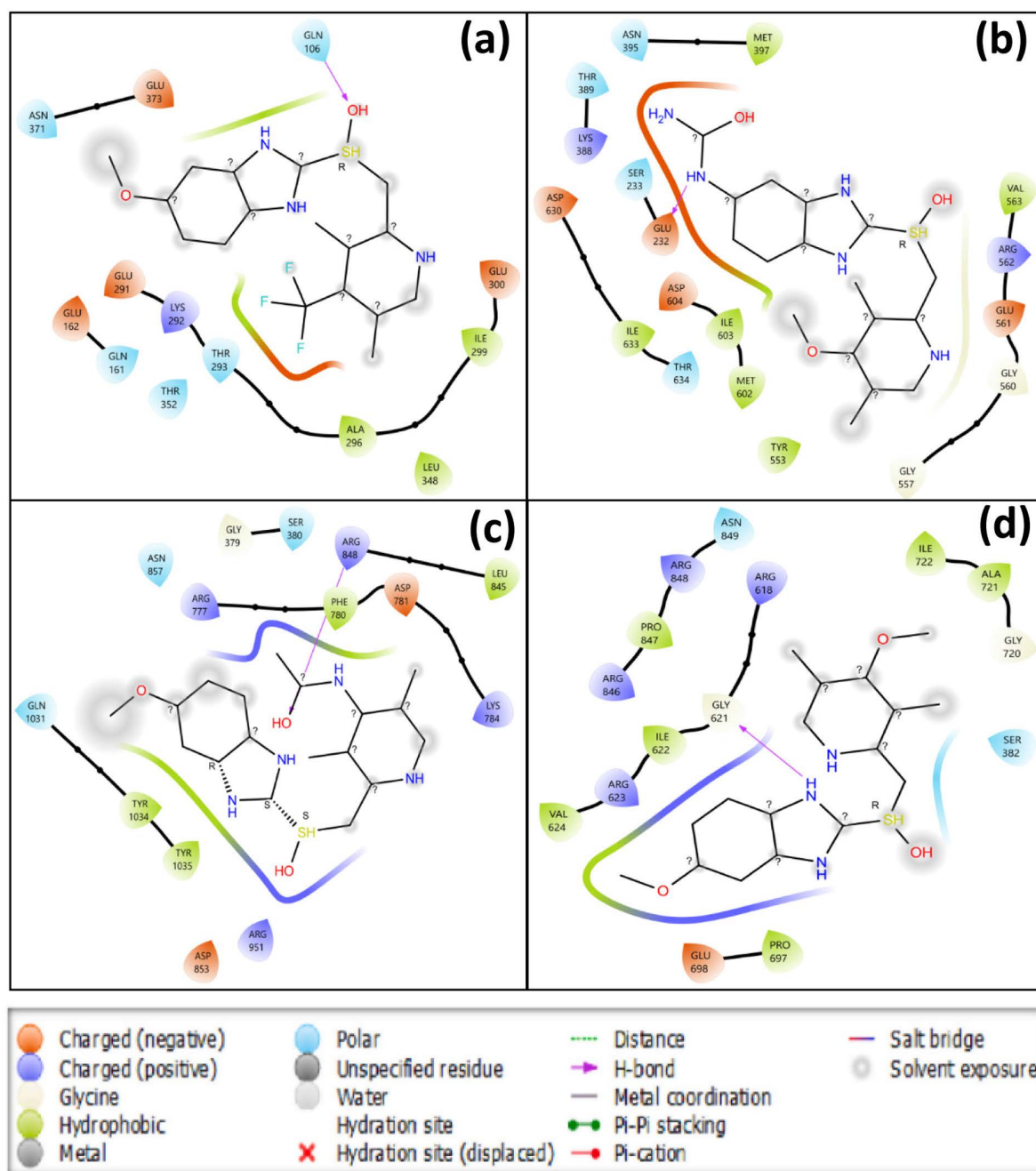
Fig 6. 2D illustration depicting the interaction between macromolecules (PTAAC1 protein) and ligands (OMP3, OMP19, OMP21, and OMP).

https://doi.org/10.1371/journal.pone.0326655.g006

3.7 ADMET prediction

In-silico ADMET screening, which includes absorption, distribution, metabolism, excretion, and toxicity, has gained increasing interest as an efficient and cost-effective alternative to *in vivo* drug testing [65,66]. **Table 4** outlines the ADMET properties of OMP and its analogues, which exhibit favourable human intestinal absorption values. However, most of

the analogues demonstrate positive outcomes for the blood-brain barrier (BBB) and could not traverse it like OMP. In addition, all the analogues have been identified as non-carcinogenic and classified as safer in terms of category III acute oral toxicity. Therefore, they pose minimal risks and are suitable for oral consumption. Most OMP analogues can easily pass through the human intestinal CACO-2 cell monolayer assay, which helps determine their permeability and likelihood of being absorbed in the intestines. As reported in the study, the drug experienced efflux back into the intestinal lumen, attributed to the presence of the P-glycoprotein transporter [67]. The drug's bioavailability is inversely affected by P-glycoprotein induction, leading to a reduction, and conversely, its inhibition results in an increase [68]. Further research suggests that suppressing P-glycoprotein could influence a drug's retention, permeability, absorption, and metabolism [69]. In our investigation, OMP and its analogues showed no P-glycoprotein inhibition. These compounds exhibit a low level of oral toxicity in the III category and do not possess carcinogenic properties, indicating that they can be considered relatively safe for oral consumption. The hERG (human ether-a-go-go-related gene) channel, which plays a vital role in cardiac regulation, can be affected by certain medications, potentially resulting in Long QT syndrome and cardiac arrhythmia [70]. The studied OMP analogues demonstrate moderate inhibition, suggesting a favourable safety profile. Around 90% of oxidative metabolic reactions are dependent on the CYP4502C9 iso-enzymes. It is important to mention that all derivatives do not act as substrates for CYP2C9, which reduces the risk of drug-drug interactions [71]. As a result, these analogues are not influenced by CYP2C9 metabolism, which decreases the chances of treatment failures.

3.8 PASS prediction

The PASS (Prediction of Activity Spectra for Substances) software predicts over 300 pharmacological effects and biochemical mechanisms by analyzing the structural formula of a substance through a robust SAR analysis of a training set with 30,000 compounds, demonstrating an approximately 86% accuracy in leave-one-out cross-validation [72,73]. From Table 5, it is evident that OMP and its analogues exhibit varying values for different properties. The analogues demonstrated significant effects in various areas, including gastric anti-secretory, anti-ulcerative, and H$^+$/K$^+$-transporting ATPase inhibition, anti-*Helicobacter pylori*, and CYP1A2 induction. These findings demonstrate that OMP3, OMP10, OMP19, and OMP21 have the most potent gastric anti-secretory and anti-ulcerative effects, respectively. In addition, OMP17 exhibits

Table 4. Absorption, distribution, metabolism, and toxicological properties (ADMET) studies of OMP and its analogues (remaining are presented in S6 Table in S1 File).

Name	Absorption			Distribution			Metabolism	Toxicity				
	HIA	HOB	C2P	BBB	P-GpI	P-GpS	CYP450 2C9	hERG	Carcinogen	AOT	RAT LD50	Hepatotoxicity
OMP	0.9968	0.8000	0.8867	-0.6326	NI(0.9680)	NS(0.5573)	NS(0.7838)	WI(0.7190)	NC(0.8318)	III	2.2254	0.6125
OMP1	0.9876	0.6375	0.8180	-0.7310	NI(0.9653)	NS(0.5296)	NS(0.7975)	WI(0.8516)	NC(0.8348)	III	2.3208	0.6375
OMP3	1.0009	0.7857	0.8340	0.541	NI(0.9063)	NS(0.5916)	NS(0.7918)	WI(0.9069)	NC(0.8115)	III	2.2909	0.6375
OMP5	0.9900	0.7714	0.7646	-0.7033	NI(0.9317)	NS(0.5259)	NS(0.8055)	WI(0.9696)	NC(0.7966)	III	2.3808	0.6375
OMP8	0.9830	0.7714	0.7112	-0.6573	NI(0.9674)	NS(0.5562)	NS(0.8459)	WI(0.7679)	NC(0.8050)	III	2.3486	0.6000
OMP11	0.9918	0.7857	0.6358	-0.6501	NI(0.9734)	S(0.56710)	NS(0.8609)	WI(0.7823)	NC(0.7711)	III	2.4562	0.5625
OMP14	0.9744	0.7286	0.5000	-0.8674	NI(0.9652)	NS(0.5666)	NS(0.8514)	WI(0.9732)	NC(0.7660)	III	2.4796	0.6125
OMP17	0.8424	0.7857	-0.5086	-0.8152	NI(0.9622)	NS(0.5302)	NS(0.7518)	WI(0.9246)	NC(0.7679)	III	2.4536	0.6250
OMP19	0.9236	0.7857	-0.5081	-0.7538	NI(0.9476)	NS(0.5610)	NS(0.7123)	WI(0.9418)	NC(0.7795)	III	2.4625	0.6586
OMP20	0.9016	0.7286	0.5197	-0.8760	NI(0.8246)	NS(0.5725)	NS(0.7938)	WI(0.9194)	NC(0.7539)	III	2.4761	0.6125
OMP21	0.9219	0.6429	0.5000	-0.6917	NI(0.8926)	NS(0.5326)	NS(0.6295)	WI(0.9107)	NC(0.7865)	III	2.4628	0.6625

Here, HIA= Human intestinal absorption, HOB= Human oral bioavailability, C2P= CACO-2 permeability, BBB= Blood brain barrier, P-GpI = P-glycoprotein inhibitor, PGpS = P-glycoprotein substrate, hERG = Human ether-a-go-go Related Gene, AOT = Acute oral toxicity, RAT LD50 (mol/kg) = Rat acute toxicity, I = inhibitor, NI = Non-inhibitor, WI = Weak inhibitor, NC = non-carcinogen, NS = Non substrate.

https://doi.org/10.1371/journal.pone.0326655.t004

the lowest inhibitory action on the H$^+$/K$^+$-transporting ATPase. Diarrhoea significantly decreases when OMP18 is introduced (from 0.850 to 0.528). In addition, OMP18 has the least impact on hepatitis, stomatitis, and depression compared to the other factors. Based on the findings, it was noted that OMP17, OMP3, OMP18, OMP19 and OMP21 display lower side effects than OMP, while OMP2, OMP4, OMP10, OMP11, OMP13, OMP1 and OMP22 manifests heightened toxicological effects in comparison. The results suggest that specific analogues OMP3, OMP19 and OMP21 demonstrate decreased toxicity compared to the OMP.

3.9 Molecular dynamics simulation analysis

To evaluate the stability and dynamic properties of the selected complexes, protein root mean square deviation (RMSD), ligand RMSD, root mean square fluctuation (RMSF), radius of gyration (rGyr), solvent accessible surface area (SASA), polar surface area (PolSA), molecular surface area (MolSA), protein-ligand interaction, and ligand-protein interaction were analyzed using MD simulation trajectory in simulation interaction diagram (SID) (Table 6). Then, hydrogen bond analysis was conducted using simulation event analysis (SEA), and post-simulation MM-GBSA analysis was calculated using the Prime MM-GBSA v3.0 of the Maestro v13.5. PCA was computed from the MD trajectories using the Bio3D package of R programming.

3.9.1 Protein root mean square deviation (RMSD) analysis. In MD simulations, RMSD is an important statistic for measuring the average deviation of atom locations over time in relation to a reference structure [74,75]. It assesses structural convergence, similarity, and stability across a 100 ns timeframe by examining specific protein constituents such as side chains, heavy atoms, backbones, and alpha carbons. RMSD also calculates ligand atom deviations when matching trajectory structures with the beginning reference over time, up to 100 ns [76]. Consequently, to examine the target protein's conformational change in the complex of the selected compound (OMP3, OMP19, OMP21) and control (OMP), as depicted in Fig 7a accordingly. After complexing to the apo-protein (PTAAC1), the RMSD average values for the selected compounds, including OMP3, OMP19, OMP21 and OMP, are 6.61 Å, 7.79 Å, 7.31 Å, and 5.29 Å, respectively, out of a total of 1001 frames. The highest RMSD values among the chosen compounds OMP3, OMP19, OMP21, and OMP are as follows: 7.834 Å, 9.085, 9.616 Å and 7.056 Å at frame numbers 855, 877, 616, and 746, respectively out of 1001. However, the lowest RMSD values and frame numbers were 1.957 Å, 2.369, 2.225 in the first frame, and 2.184 Å in the second frame for the selected compounds OMP3, OMP19, OMP, and OMP21, respectively. The compounds (OMP3 and OMP19), when compared to the control (OMP) in Fig 7a, demonstrated better stability with

Table 5. PASS predicted data of OMP and its analogues (Pa values, indicating to be active) (remaining are presented in S7 Table in S1 File).

Name	Gastric Anti-secretory	Anti-ulcerative	H+/K+-transporting ATPase inhibitor	Anti-Helicobacter Pylori	CYP1A2 inducer	Nephritis	Hepatitis	Stomatitis	Depression	Diarrhea
OMP	0.969	0.942	0.922	0.937	0.888	0.842	0.847	0.864	0.842	0.850
OMP1	0.823	0.892	0.893	0.893	0.940	0.851	0.800	0.833	0.902	0.820
OMP2	0.910	0.874	0.884	0.828	0.955	0.897	0.908	0.911	0.959	0.892
OMP3	0.700	0.767	0.734	0.670	0.872	0.830	0.711	0.839	0.904	0.709
OMP5	0.717	0.857	0.836	0.900	0.843	0.881	0.783	0.857	0.722	0.546
OMP8	0.777	0.838	0.767	0.771	0.907	0.861	0.846	0.862	0.924	0.846
OMP11	0.852	0.906	0.726	0.816	0.933	0.852	0.866	0.896	0.911	0.858
OMP14	0.864	0.872	0.738	0.807	0.950	0.891	0.888	0.914	0.958	0.862
OMP17	0.841	0.828	0.476	0.740	0.869	0.771	0.621	0.687	0.737	0.607
OMP19	0.971	0.930	0.709	0.797	0.935	0.858	0.834	0.880	0.817	0.837
OMP20	0.736	0.825	0.524	0.851	0.958	0.864	0.780	0.735	0.802	0.820
OMP21	0.903	0.826	0.559	0.638	0.707	0.735	0.626	0.721	0.698	0.566

https://doi.org/10.1371/journal.pone.0326655.t005

a slightly higher fluctuation at a simulation time range of 0 ns to 15 ns and maintained constant fluctuation with minimal conformational changes between 15 ns to 100 ns. On the other hand, during the simulation time range of 0-70 ns and 0-50 ns, the compound OMP21 and OMP showed comparatively high fluctuation and maintained the lowest continuous fluctuation from 70-100 ns and 50-100 ns, respectively.

3.9.2 Ligand RMSD analysis. The Ligand RMSD is a useful method for evaluating conformational changes and ligand stability inside a binding pocket, and RMSD fluctuations indicate possible destabilization or conformational changes [75,77]. The complex docking structure was first aligned with the reference protein backbone to determine the RMSD of the selected compounds OMP3, OMP19, OMP21, and OMP in Fig 7b. The average ligand RMSD values for these compounds, OMP3, OMP19, OMP21, and OMP, were 2.26 Å, 0.96 Å, 0.97 Å, and 1.52 Å, respectively. In the analysis of the chosen compounds, OMP3, OMP19, OMP21, and OMP exhibited lower ligand RMSD values of 0.85, 0.39, 0.249, and 0.514 at frame numbers 4, 120, 1, and 1, respectively. The highest possible values were 2.596, 1.99, 2.731, and 2.799 at frames 505, 12, 849, and 995, respectively. OMP19 and OMP21 had lower average ligand RMSD values than the control, indicating that they are more stable in binding, structural integrity, and prediction accuracy.

3.9.3 Root mean square fluctuation (RMSF) analysis. The RMSF values measure the local variations and stability of amino acid (AA) residues in a complex system [77]. Therefore, as shown in Fig 7c, the RMSF values of the compounds OMP3, OMP19, OMP21, and OMP in the complex were assessed to ascertain how protein structural flexibility changes when particular compounds attach to a particular residual position. Specifically, the average RMSF values for OMP3, OMP19, OMP21, and control OMP are 2.2 Å, 2.01 Å, 2.4 Å, and 2.3 Å, respectively. These values are concentrated around 2-3 Å [78], indicating the different levels of flexibility in different regions of the protein structure. The selected three

Table 6. Using a 100 ns molecular dynamics simulation, three lead compounds (OMP3, OMP19, OMP21) and the control drug (OMP) produced varying parameters, including the highest (H), lowest (L), and average (A).

Parameter	Value	OMP	OMP3	OMP19	OMP21
Protein Cα RMSD	H. RMSD (Å)	7.056	7.834	9.085	9.616
	L. RMSD (Å)	2.225	1.957	2.369	2.184
	A. RMSD (Å)	5.290	6.610	7.790	7.310
Ligand RMSD	H. L-RMSD (Å)	2.799	2.596	1.990	2.731
	L. L-RMSD (Å)	0.514	0.850	0.390	0.249
	A. L-RMSD (Å)	1.520	2.260	0.960	0.970
Protein Cα RMSF	H. RMSF (Å)	18.480	11.08	16.461	26.762
	L. RMSF (Å)	0.875	0.827	0.775	1.051
	A. RMSF (Å)	2.300	2.200	2.010	2.400
Radius of gyration	H. rGyr (Å)	4.763	4.950	5.225	5.142
	L. rGyr (Å)	3.686	4.111	4.535	3.858
	A. rGyr (Å)	4.470	4.730	4.990	4.830
Solvent-accessible surface area (SASA)	H. SASA($Å^2$)	515.429	215.938	417.039	237.023
	L. SASA ($Å^2$)	166.864	26.003	145.449	68.267
	A. SASA ($Å^2$)	352.090	89.670	279.42	144.160
Molecular surface area (MolSA)	H. MolSA ($Å^2$)	337.378	338.173	354.792	363.022
	L. MolSA ($Å^2$)	313.131	324.639	334.055	335.158
	A. MolSA ($Å^2$)	329.400	332.070	346.370	354.450
Polar surface area (PolSA)	H. PolSA ($Å^2$)	124.205	111.134	232.288	156.923
	L. PolSA ($Å^2$)	82.502	81.661	198.183	110.524
	A. PolSA ($Å^2$)	105.450	96.450	218.500	139.630
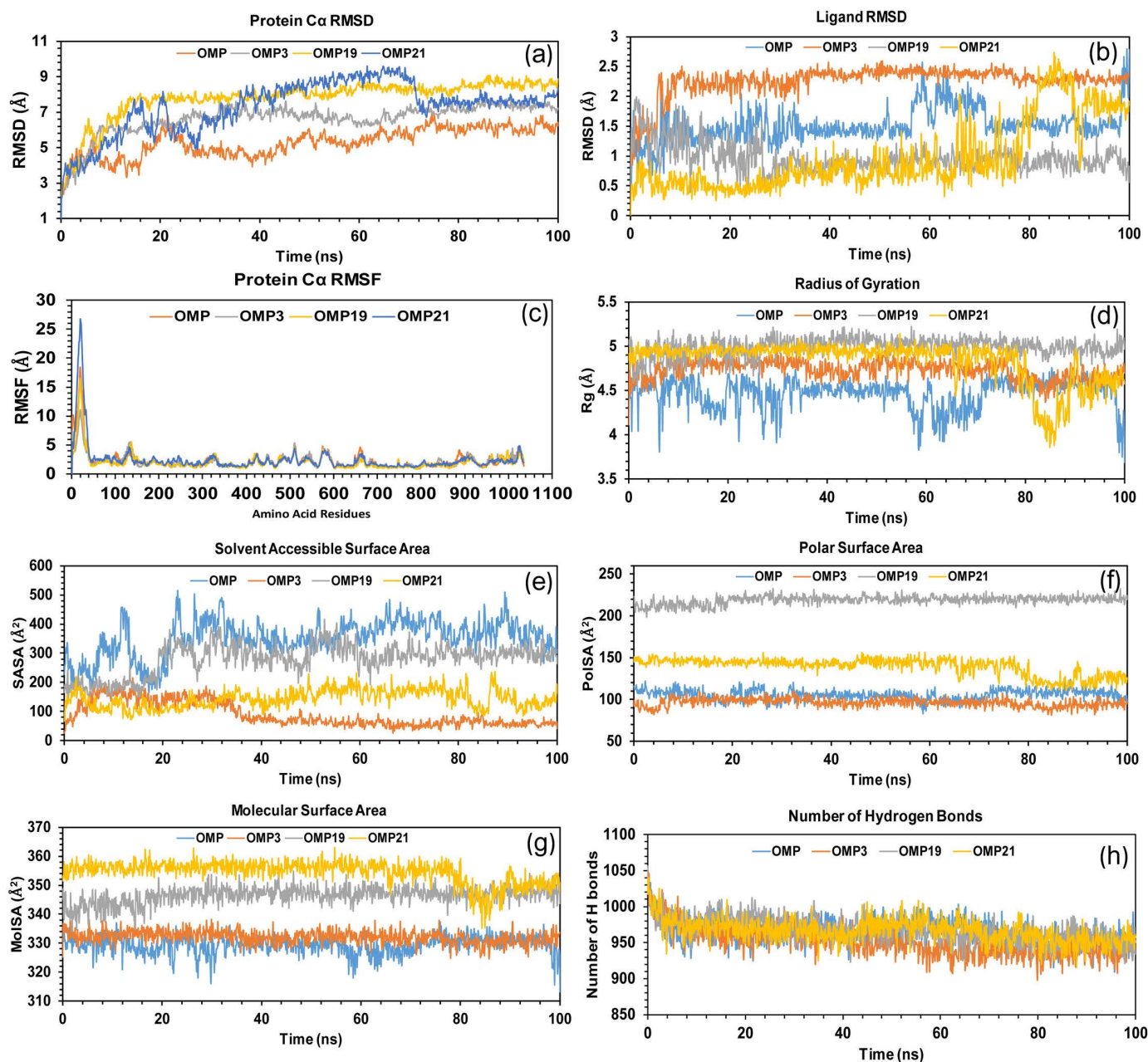
Fig 7. The protein RMSD (a), Ligand RMSD (b), RMSF (c), rGyr (d), SASA (e), PolSA (f), MolSA (g), and Hydrogen bond (h) analyses are displayed for three selected compounds (OMP3, OMP19, OMP21) and OMP (control); derived from the MD simulation.

compounds OMP3, OMP19, OMP21, and control OMP had the following RMSF values: the lowest values were 0.827 Å, 0.775 Å, 1.051 Å, and 0.875 Å, respectively, at residual positions LYS793, TYR789, and MET602; the highest values were 11.08 Å, 16.461 Å, 26.762 Å, and 18.48 Å, respectively, at residual positions GLY19. Fig 7c shows a peak region of the protein for each of the chosen compounds. During the simulation period, these residue positions-which included GLY133, ARG510, LYS574, LEU659, and ARG1022 exhibited the most fluctuations. Based on the RMSF, it was discovered that the

stiffest secondary structural elements, like alpha-helices and beta-sheets, have at least 150 to 500 AA and 600 to 1040 AA residues.

3.9.4 Radius of gyration (rGyr) analysis.

The radius of gyration (rGyr) measures the root mean square distance of a molecule's atoms from its center of mass and is used in MD simulations to quantify the compactness or overall shape of a molecule, especially proteins and chemical compounds. Throughout the 100 ns simulation period, the stability of the chosen compounds OMP3, OMP19, OMP21, and OMP interacting with the target protein was assessed using rGyr in Fig 7d. The minimum rGyr values recorded for OMP3, OMP19, OMP21, and OMP were 4.111 Å, 4.535 Å, 3.858 Å, and 3.686 Å at frame numbers 1, 17, 849, and 1000, respectively. Conversely, the peak values recorded were 4.95 Å, 5.225 Å, 5.142 Å, and 4.763 Å at frame numbers 517, 570, 547, and 771, as well. Additionally, the average rGyr values for OMP3, OMP19, OMP21, and OMP were found to be 4.73 Å, 4.99 Å, 4.83 Å, and 4.47 Å, respectively. Fig 7d depicts the OMP as a compact and sturdy structure, serving as a benchmark for comparison. The OMP3 curve closely resembles the OMP, with somewhat higher rGyr values while retaining a similar level of compactness and stability, implying minimal structural expansion. Similarly, the OMP19 curve exhibits a slight stabilization above the OMP3 and OMP, indicating a moderate level of compactness with only minimal variations from the OMP. The OMP21 curve shows the highest rGyr values, indicating a bit less compactness and greater flexibility; nonetheless, the overall trend stays pretty aligned with the control. The findings suggest that the structural compactness of our systems aligns closely with the OMP, exhibiting only minor variations that remain within the bounds of benchmark stability.

3.9.5 Solvent accessible surface area (SASA) analysis.

SASA is the surface area where the solvent molecules and the protein or ligand come into contact. The simulation analysis shows a correlation with the solvent-complex interactions [79]. The SASA value determines the magnitude and significance of the protein arrangement changes that occur when a ligand attaches to a receptor [80]. A greater SASA value indicates a larger protein volume, and minimal variation is expected during the simulation time [81]. The SASA values for OMP3, OMP19, OMP21, and OMP are determined in Fig 7e. The minimum values recorded for these compounds were 26.003 Å², 145.449 Å², 68.267 Å², and 166.864 Å² in frames 1, 50, 1, and 172, respectively. The highest values for OMP3, OMP19, OMP21, and OMP compounds were 215.938 Å², 417.039 Å², 237.023 Å², and 515.429 Å² in frame numbers 139, 528, 874, and 230, respectively. In frame numbers 139, 528, 874, and 230, OMP3, OMP19, OMP21, and OMP molecules had the greatest values of 215.938 Å², 417.039 Å², 237.023 Å², and 515.429 Å², respectively. The average SASA values for OMP3, OMP19, OMP21, and OMP were 89.67 Å², 279.42 Å², 144.16 Å², and 352.09 Å², respectively. The complicated mechanism had an average SASA value ranging from 85 to 355 Å², indicating that an AA residue was easily accessible to the molecule. The OMP has the greatest SASA values (300–500 Å²). This means that it is the most solvent-exposed and contains fewer interactions or structures. The other compounds (OMP3, OMP19, and OMP21) have substantially lower SASA values, showing that they are either more compact or have stronger interactions to limit surface exposure. OMP19 has SASA values that are slightly reduced compared to OMP (200–400 Å²); in contrast, OMP21 and OMP3 consistently demonstrate the lowest SASA, remaining below 200 Å², which suggests reduced exposure. This indicates that the OMP3, OMP19, and OMP21 molecules exhibit a greater binding potential or enhanced structural stability than OMP.

3.9.6 Polar surface area (PolSA) and molecular surface area (MolSA) analyses.

The PolSA and MolSA tests reveal that the chosen compounds; OMP3, OMP19, OMP21, and OMP maintain their stable surface properties during the 100 ns simulation. OMP3 has a slightly higher PolSA of 111.134 Å² and the highest MolSA of 338.173 Å², indicating strong polar surface exposure. OMP19's high PolSA (198-235 Å²) and MolSA (354.792 Å²) indicate a larger surface area.OMP21 exhibits a high PolSA of 110-156 Å² and MolSA of 363.022 Å², indicating a compact structure with a low polar surface area. The simulation showed minimal MolSA and PolSA variations for all systems. This demonstrated the structure's stability and the surface's constant exposure without any significant shape changes. OMP19 and OMP21 exhibit the highest average PolSA (218.50 Å² and 139.63 Å²) and the largest average MSA (346.37 Å² and 354.45 Å²) compared to

OMP (PolSA at 105.45 Å² and MolSA at 329.40 Å²), indicating extensive surface exposure in Fig 7f and 7g. OMP3 has a less compact structure than other compounds, with an average MolSA of 332.08 Å² and a lower PolSA of 96.45 Å². All systems had consistent MolSA and PolSA values, indicating structural stability throughout the experiment. The simulation revealed that all systems had modest MolSA and PolSA variances.

3.9.7 Hydrogen bond analysis. Hydrogen bonds (HB), a form of noncovalent contact, substantially influence biomolecule behaviour and three-dimensional structure [82]. The biological recognition process depends on hydrogen bonding, and the molecular dynamics required for biological processes are inextricably linked to the rapid production and breakdown of hydrogen bonds [83]. Hydrogen bonds are required to stabilize the ligand with the target protein, aid in adsorption, accelerate metabolic processes, and improve therapeutic selectivity [76,84,85]. Fig 7h depicts the monitoring of H-bond formation in the protein-ligand complex interaction over a 100 ns simulated period. Consequently, Fig 7h illustrates the number of H-bonds established throughout the interaction of the protein-ligand complex during the 100 ns simulation. The average H-bond numbers for the selected compounds, which include OMP3, OMP19, OMP21, and OMP, were found to be 950.69, 966.88, 965.63, and 964.20, respectively. Throughout the simulation, each compound formed hydrogen bonds ranging from 895 to 1020 simultaneously. The connection between the ligand and receptor will experience significant enhancement and stabilization.

3.9.8 Protein-ligand and ligand-protein contact analysis. We used the simulated interactions diagram (SID) to study the complex structure of a protein, its associated ligands, and their molecular interactions over a 100-ns simulation period. In Fig 8, several characteristics, such as H-bonds, ionic, hydrophobic, and water bridge bonds, were used to investigate and demonstrate the interactions between the protein and selected compounds. During the 100 ns simulation, the interactions between each molecule resulted in a stable binding to the target macromolecule. More than two contacts were found in OMP3, with interaction fractions of 0.20, 1.90, 0.28, 0.12, 0.11, and 1.10 for residues LYS31, ARG105, GLN106, GLU162, LYS292, and GLU373, in that order. The particular connection consistently results from the same subtype repeatedly engaging with the ligand throughout the simulation, as shown in Fig 8a. OMP19 had substantial interactions with GLU234 (0.28), GLU653 (1.5), VAL663 (0.55), and ARG668 (0.1), which occurred at optimal times throughout the simulation (Fig 8b). The compound OMP21 established several interactions with the residues ASP853 (0.3), ASN857 (0.2), ARG951 (1.3), TYR1034 (0.8), and TYR10354 (0.1), and the simulation duration effectively preserved these connections (Fig 8c). The simulation time for compound OMP effectively captured various interactions at residues LYS669 (0.2), ASP670 (1.35), ARG694 (0.05), ARG846 (0.1), and ASN (0.03) (Fig 8d). Nonetheless, OMP3 demonstrates a notable interaction involving hydrogen and other bonds with the PTAAC1, as illustrated in Fig 9a.

The simulated interactions diagram (SID) illustrates the protein interactions among the chosen compounds, OMP3, OMP19, OMP21, and OMP, in Fig 9. In contrast to OMP, OMP3 and OMP21 exhibited significant interaction residues (exceeding two) throughout the simulation. This led to several interactions with the identical subtype of ligand, thus maintaining the distinct interaction. The study demonstrated enhanced stability in the interaction between the ligand and protein.
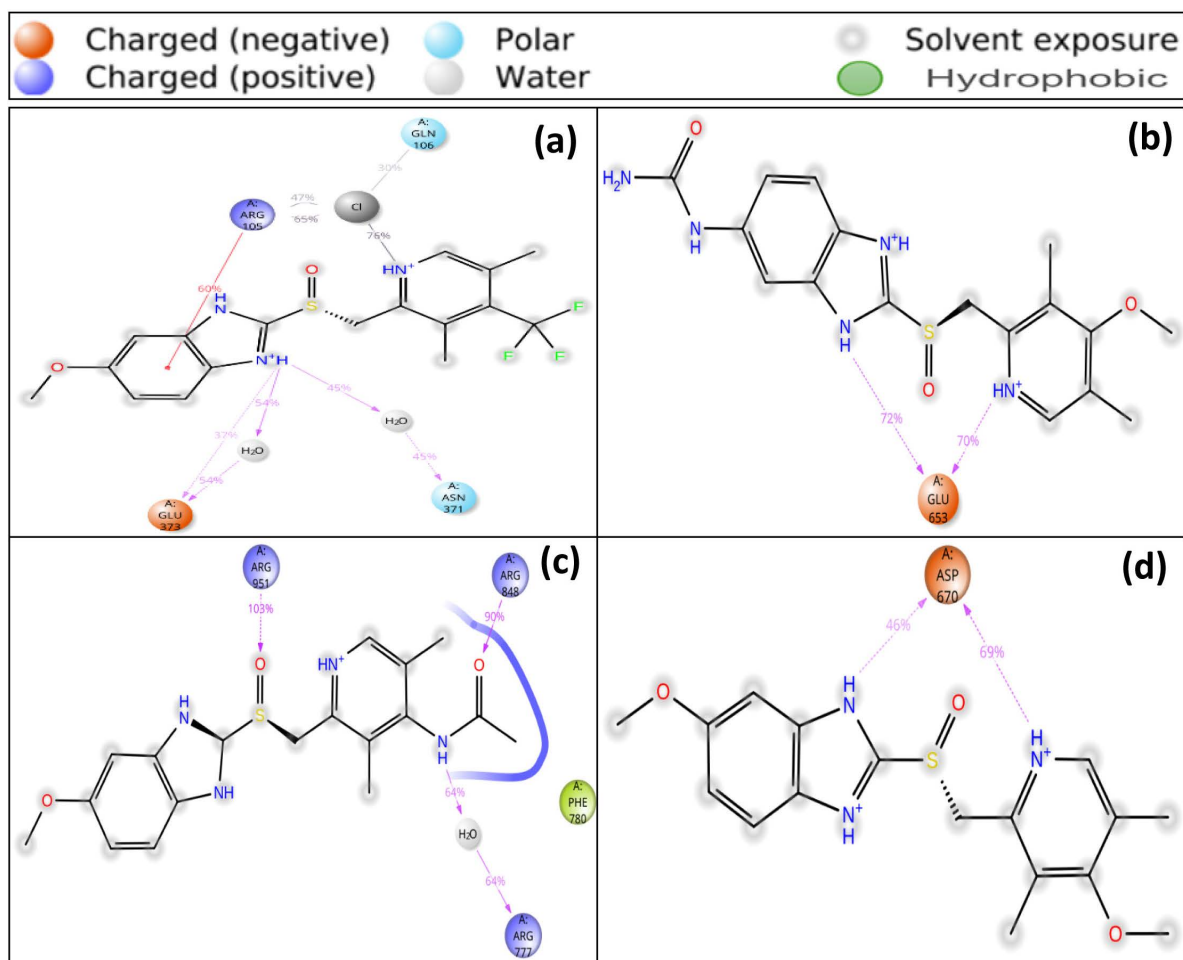
3.9.10 Principal component analysis (PCA) analysis. Principal component analysis is a method for reducing dimensionality that might be useful in studying protein structures and dynamics. The protein-ligand complexes' conformational dynamics were examined using Principal Component Analysis (PCA) applied to the trajectories obtained from molecular dynamics (MD) simulations. Fig 10 shows the principal component analysis results for the OMP3, OMP19, and OMP21 complexes, as well as the OMP complex. The first three PCs accounted for a significant portion of the OMP3 complex's overall mobility (Fig 10a). Of the total variation, PC1 was responsible for 36.19 %, PC2 for 16.19 %, and PC3 for 12.8%. Following PC1, the eigenvalue plot displayed a steep decline, indicating that the primary motions were primarily caused by the first principal component. In Fig 10b, we can see that the OMP19 complex showed more conformational variation along PC1, which explained 45.18 % of the total variance,
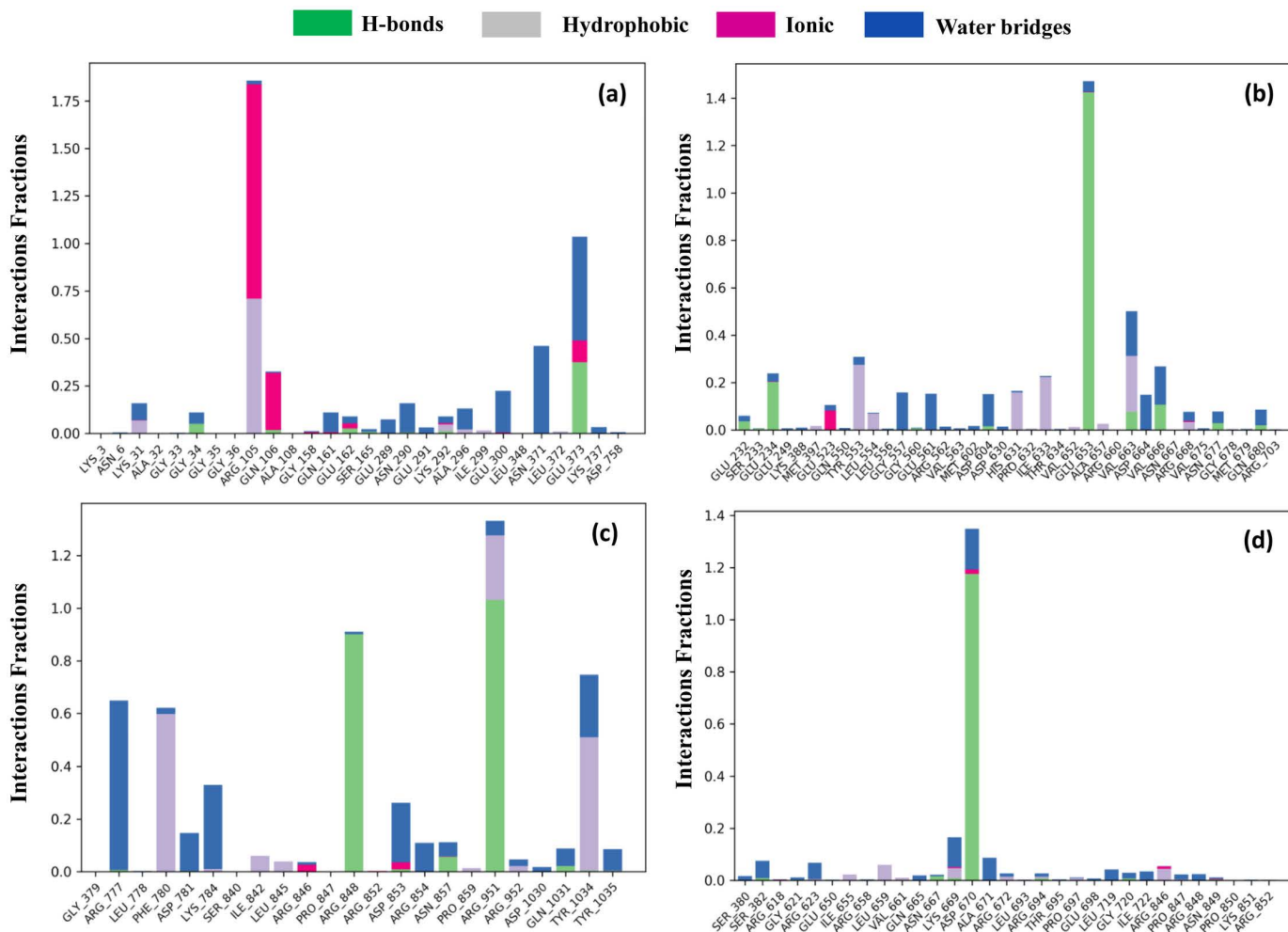
Fig 8. The grouped bar charts show the protein-ligand interactions identified during the 100 ns simulation of PTAAC1 protein binding with OMP3 (a), OMP19 (b), OMP21 (c) and OMP (control) (d).

https://doi.org/10.1371/journal.pone.0326655.g008

compared to 14.77 % along PC2 and 7.55 % along PC3. In comparison to OMP3, OMP19's eigenvalue plot showed a more gradual decline, indicating somewhat more dispersed dynamic behaviour over several modes. Fig 10c shows the OMP21 complex, where the first principal component (PC1) accounted for almost half of the overall motion, explaining 50.65% of the variance. Two-thirds of the variation was explained by PC2, while the remaining 6.51% was explained by PC3. For OMP21, the more precipitous decline in eigenvalues following PC1 suggests a more consistent and dominating motion along a single mode. Within the control OMP complex (Fig 10d), PC1 accounted for 45.18% of the variance, PC2 for 16.94%, and PC3 for 12.04%. The eigenvalue distribution showed that OMP3 and OMP19 were behaving in an intermediate manner with regard to motion spread. The comparison's findings showed that the OMP21 complex exhibited the most consistent dynamic behaviour. The fact that conformations were more closely packed along the main components and that PC1 recorded the highest variance—50.65%—supported this. OMP19's movement was more widely distributed among numerous PCs, suggesting greater flexibility, whereas OMP3's movement was more spread throughout the initial three PCs. The OMP complex showed moderate stability but somewhat greater dispersion when compared to OMP21. PC1 typically exhibits the most significant variance,

Fig 9. Analysis of protein-ligand interactions displayed from a 100 ns simulation of the PTAAC1 protein binding with OMP3 (a), OMP19 (b), OMP21 (c) and OMP (control) (d).

https://doi.org/10.1371/journal.pone.0326655.g009

with a reduction in variation observed as we progress through the principal components, suggesting more restricted and localized movements. Distinct conformational variations were observed through a simple clustering approach in the PC subspace. The colours red and white represent the lowest and moderate levels of movement, respectively, whereas blue signifies the highest degree.

3.9.11 Post-simulation MM-GBSA analysis. MM-GBSA techniques have been used in this study to compute the binding free energy of the protein of interest in complex with the ligand. Following each 50 ns molecular dynamics simulation, the 100 ns dynamic simulation trajectory was utilized to compute the MM-GBSA for the protein-ligand complex structure. Upon complexation with the targeted protein, the initial (0 ns), intermediate (50 ns), and final (100 ns) negative binding free energy (dG Bind) values for OMP3, OMP19, OMP21, and OMP were recorded as follows: -26.67, -27.74, and -36.91 kcal/mol; -39.67, -22.10, and -26.45 kcal/mol; -64.67, -46.96, and -12.61 kcal/mol; -25.76, -19.87, and -15.02 kcal/mol, respectively (Table 7). Therefore, the selected compounds should be able to bind to the target protein for an extended period.
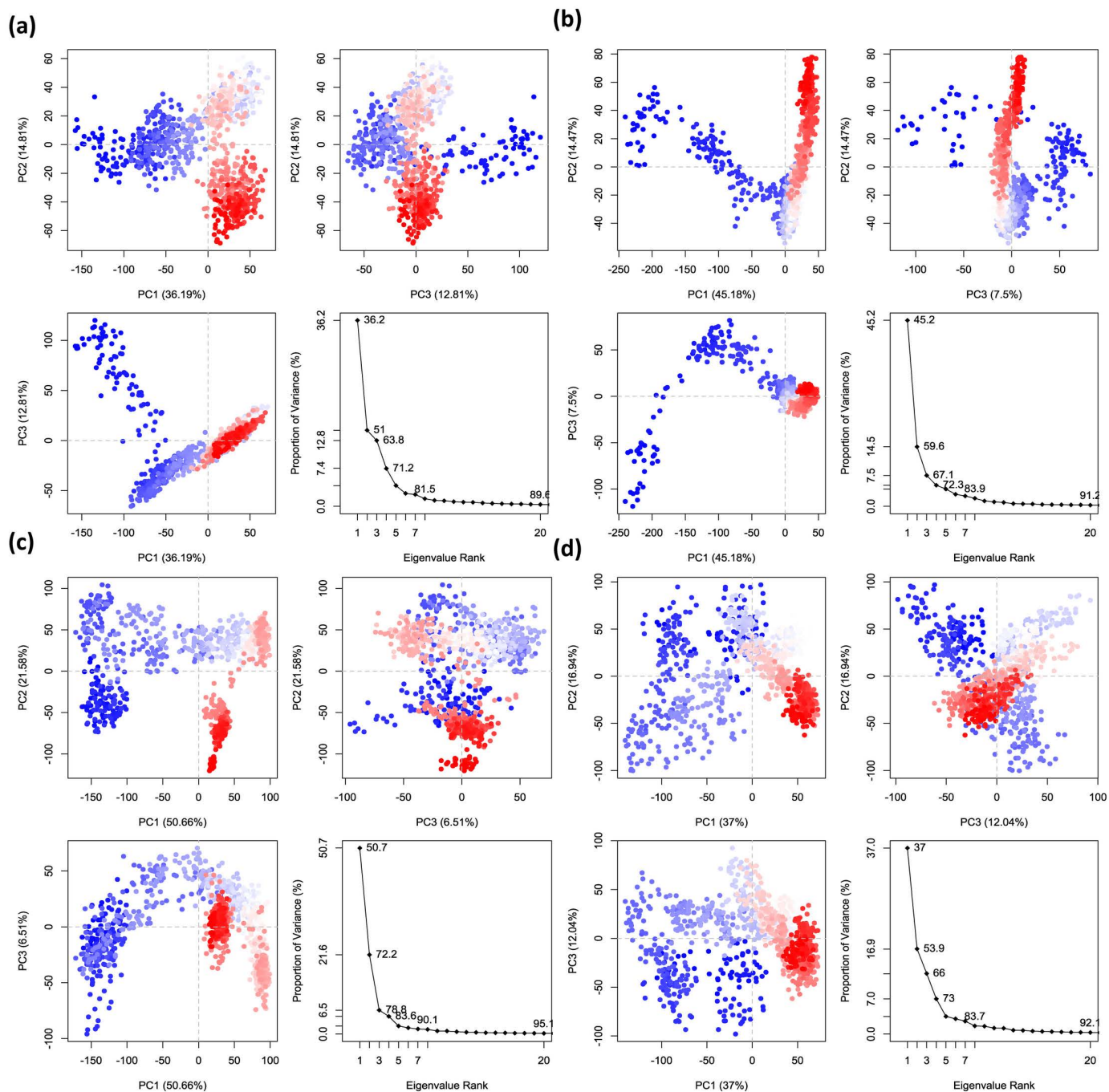
Fig 10. Eigenvalues in principal component analysis vs proportion of variance. Each region is displayed on three independent panels. There are three different versions: PC1, PC2, and PC3. In this scenario, the compounds are OMP3 (a), OMP19 (b), OMP21 (c), and OMP (control) (d).

https://doi.org/10.1371/journal.pone.0326655.g010

Table 7. The table depicts the MM-GBSA binding energy components for OMP3, OMP19, OMP21, and OMP (control) with the target protein at initial, intermediate, and final production.

Time	dG Bind	dG Bind Coulomb	dG Bind Covalent	dG Bind Hbond	dG Bind Lipophilicity	dG Bind Packing	dG Bind Solvation Generalized Born	dG Bind Van Der Waals
MM-GBSA of OMP								
0 ns	-25.760	90.724	3.046	-0.100	-6.197	-1.178	-81.304	-30.751
50 ns	-19.875	4.292	2.080	-0.547	-4.917	0.000	-1.080	-19.703
100 ns	-15.024	1.934	0.671	-0.201	-3.170	-2.548	0.992	-12.704
MM-GBSA of OMP3								
0 ns	-26.667	-9.238	1.493	-0.478	-8.253	-5.974	46.176	-50.394
50 ns	-27.742	-7.345	2.538	-0.998	-8.175	-7.418	39.571	-45.915
100 ns	-36.914	-11.680	3.279	-1.116	-8.111	-7.476	36.033	-47.842
MM-GBSA of OMP19								
0 ns	-39.672	9.466	2.503	-3.906	-9.055	-0.069	6.059	-44.671
50 ns	-22.104	19.073	0.398	-1.797	-2.972	-3.873	-11.414	-21.519
100 ns	-26.449	-1.118	4.516	-2.025	-3.781	-1.744	7.246	-29.543
MM-GBSA of OMP21								
0 ns	-64.551	-34.526	5.591	-3.385	-17.805	-1.628	39.951	-52.750
50 ns	-46.957	-25.684	2.397	-1.716	-13.071	-0.653	30.876	-39.105
100 ns	-12.610	-1.418	5.424	-1.474	-10.492	-1.002	32.474	-36.122

https://doi.org/10.1371/journal.pone.0326655.t007

4 Conclusion

To summarize, this study unveils the discovery of new compounds through structural modifications, resulting in a wide range of alterations in physicochemical, biological, and pharmacokinetic properties through the incorporation of various functional groups. Certain alterations have been found to affect the dipole moment and free energy of many analogues. Thermodynamic studies evaluate the chemical, dielectric, and chemical durability, whereas UV-Vis spectral analysis visually depicts electronic transition spectra and absorption of the analogues at different wavelengths. In addition, FT-IR spectrum analysis offers information on the vibrational modes of analogues and, most significantly, identifies the presence of various functional groups in the molecular structure of the analogues. Nonbonding interactions, such as hydrogen and hydrophobic bonds, make certain analogues an effective therapeutic candidate. The ideal bond distances seen in many analogues are further strengthened by strong hydrogen bonding, raising affinity and highlighting the significance of nonbonding interactions in drug stability. After undertaking ADMET and PASS predictions on all analogues, it was ultimately determined that certain OMP analogues outperformed the control. Furthermore, the results of molecular docking, interactions, MD simulation, and principal component analysis make it evident that a few analogues, such as OMP3 and OMP21, exhibit better binding affinities to the targeted protein PTAAC1 than OMP. These in silico analyses serve as valuable tools in preclinical research, providing insights into advancing the development of a modified version of the primary studied drug with improved properties. However, experimental validation is necessary to verify potency, toxicity, off-target effects, and other pharmacokinetic and pharmacodynamic properties of these novel OMP analogues. Prospectively, validating these preclinical profiles will necessitate undertaking *in vivo* and *in vitro* experiments to bridge computational predictions with therapeutic significance.

Supporting information

S1 File. **S1 Table.** Chemical structure and IUPAC name of the OMP and its analogues. **S1 Fig.** Optimized chemical structure of OMP and its analogues. **S2 Fig.** Molecular orbitals (HOMO and LUMO) and HUMO-LOMO energy gap of OMP and its analogues. **S3 Fig.** Free energies (Hartree) (a), dipole moments (Debye) (b), HOMO-LUMO gaps (c), and

chemical softness (d) of OMP and its analogues. **S2 Table.** Energy (eV) of HOMO-LUMO, gap, hardness (η), softness (S), chemical potential (μ), electronegativity (χ), and electrophilicity (ω) of OMP, and its analogues. **S4 Fig.** Electrostatic potential map of OMP analogues. **S5 Fig.** FT-IR spectra of OMP analogues. **S6 Fig.** UV-vis spectra of OMP analogues. **S3 Table.** Vibrational frequencies of OMP analogues. **S4 Table.** UV-vis spectral data of OMP and its analogues. **S7 Fig.** Binding energy of OMP and its analogues with the targeted PTAAC1 protein. **S5 Table.** Binding affinity and nonbonding interactionss of remaining compounds with the PTAAC1 protein. **S8 Fig.** Superimposed view of the docked conformer with the targeted protein, non-bonding interactions, and the hydrogen bond surface of OMP and its analogues. **S6 Table.** Absorption, distribution, metabolism, and toxicological properties (ADMET) studies of OMP analogues. **S7 Table.** PASS predicted data of OMP analogues.
(DOCX)

S2 File. Protein RMSD.
(XLSX)

S3 File. Protein RMSF.
(XLSX)

S4 File. Ligand properties and H bonds.
(XLSX)

S5 File. Post-simulation MM-GBSA.
(XLSX)

Acknowledgement

Author contributions

Conceptualization: Monir Uzzaman.

Data curation: Mahmudul Hasan, Md. Ifteker Hossain, Noimul Hasan Siddiquee, Ezaz Ahmed, Md Rahamatolla, Tasrin Nahar, Popy Rani Paul, Mahmudul Hassan Suhag.

Formal analysis: Mahmudul Hasan, Md. Ifteker Hossain, Noimul Hasan Siddiquee, Ezaz Ahmed, Md Walid Hossain Talukder.

Investigation: Mahmudul Hassan Suhag, Monir Uzzaman.

Methodology: Mahmudul Hasan, Md. Ifteker Hossain, Noimul Hasan Siddiquee, Ezaz Ahmed, Md Walid Hossain Talukder, Md Rahamatolla, Tasrin Nahar, Popy Rani Paul, Monir Uzzaman.

Project administration: Monir Uzzaman.

Resources: Mahmudul Hasan, Md. Ifteker Hossain, Noimul Hasan Siddiquee.

Software: Mahmudul Hasan, Md. Ifteker Hossain, Noimul Hasan Siddiquee.

Supervision: Monir Uzzaman.

Validation: Mahmudul Hasan, Md. Ifteker Hossain, Noimul Hasan Siddiquee, Ezaz Ahmed, Monir Uzzaman.

Visualization: Mahmudul Hasan, Md. Ifteker Hossain, Noimul Hasan Siddiquee, Ezaz Ahmed, Md Walid Hossain Talukder.

References

1. Clarrett DM, Hachem C. Gastroesophageal Reflux Disease (GERD). Mo Med. 2018;115:214. https://doi.org/10.1016/B978-0-443-13911-6.00025-6

2. Mermelstein J, Mermelstein AC, Chait MM. Proton pump inhibitors for the treatment of patients with erosive esophagitis and gastroesophageal reflux disease: current evidence and safety of dexlansoprazole. Clin Exp Gastroenterol. 2016;9:163–72. https://doi.org/10.2147/CEG.S91602 PMID: 27471402

3. Shin JM, Sachs G. Pharmacology of proton pump inhibitors. Curr Gastroenterol Rep. 2008;10(6):528–34. https://doi.org/10.1007/s11894-008-0098-4 PMID: 19006606

4. Brett S. Science review: The use of proton pump inhibitors for gastric acid suppression in critical illness. Crit Care. 2005;9(1):45–50. https://doi.org/10.1186/cc2980 PMID: 15693983

5. Jain KS, Shah AK, Bariwal J, Shelke SM, Kale AP, Jagtap JR, et al. Recent advances in proton pump inhibitors and management of acid-peptic disorders. Bioorg Med Chem. 2007;15(3):1181–205. https://doi.org/10.1016/j.bmc.2006.07.068 PMID: 17150362

6. Marks SL, Kook PH, Papich MG, Tolbert MK, Willard MD. ACVIM consensus statement: Support for rational administration of gastrointestinal protectants to dogs and cats. J Vet Intern Med. 2018;32(6):1823–40. https://doi.org/10.1111/jvim.15337 PMID: 30378711

7. Freedberg DE, Lebwohl B, Abrams JA. The impact of proton pump inhibitors on the human gastrointestinal microbiome. Clin Lab Med. 2014;34(4):771–85. https://doi.org/10.1016/j.cll.2014.08.008 PMID: 25439276

8. Hu Z-H, Shi A-M, Hu D-M, Bao J-J. Efficacy of proton pump inhibitors for patients with duodenal ulcers: A pairwise and network meta-analysis of randomized controlled trials. Saudi J Gastroenterol. 2017;23(1):11–9. https://doi.org/10.4103/1319-3767.199117 PMID: 28139495

9. Poitras P, Gingras M-H, Rehfeld JF. The Zollinger-Ellison syndrome: dangers and consequences of interrupting antisecretory treatment. Clin Gastroenterol Hepatol. 2012;10(2):199–202. https://doi.org/10.1016/j.cgh.2011.08.012 PMID: 21871248

10. Shi S, Klotz U. Proton pump inhibitors: an update of their clinical use and pharmacokinetics. Eur J Clin Pharmacol. 2008;64(10):935–51. https://doi.org/10.1007/s00228-008-0538-y PMID: 18679668

11. Shin JM, Kim N. Pharmacokinetics and pharmacodynamics of the proton pump inhibitors. J Neurogastroenterol Motil. 2013;19(1):25–35. https://doi.org/10.5056/jnm.2013.19.1.25 PMID: 23350044

12. Caro JJ, Salas M, Ward A. Healing and relapse rates in gastroesophageal reflux disease treated with the newer proton-pump inhibitors lansoprazole, rabeprazole, and pantoprazole compared with omeprazole, ranitidine, and placebo: evidence from randomized clinical trials. Clin Ther. 2001;23(7):998–1017. https://doi.org/10.1016/s0149-2918(01)80087-4 PMID: 11519776

13. Carabotti M, Annibale B, Lahner E. Common Pitfalls in the Management of Patients with Micronutrient Deficiency: Keep in Mind the Stomach. Nutrients. 2021;13(1):208. https://doi.org/10.3390/nu13010208

14. Rowbotham DJ, Kimpson PM, Thompson HM. Gut motility and secretions. Foundations of Anesthesia. Elsevier; 2006. 739–51. https://doi.org/10.1016/b978-0-323-03707-5.50067-x

15. De Giorgi F, Palmiero M, Esposito I, Mosca F, Cuomo R. Pathophysiology of gastro-oesophageal reflux disease. Acta Otorhinolaryngol Ital. 2006;26:241. https://doi.org/10.1097/00020840-199402000-00016

16. Shanika LGT, Reynolds A, Pattison S, Braund R. Proton pump inhibitor use: systematic review of global trends and practices. Eur J Clin Pharmacol. 2023;79(9):1159–72. https://doi.org/10.1007/s00228-023-03534-z PMID: 37420019

17. Adelman AM, Lewis PR. Gastritis, Esophagitis, and Peptic Ulcer Disease. Family Medicine. Springer International Publishing; 2014. 1–9. https://doi.org/10.1007/978-1-4939-0779-3_94-1

18. Shanika LGT, Reynolds A, Pattison S, Braund R. Proton pump inhibitor use: systematic review of global trends and practices. Eur J Clin Pharmacol. 2023;79(9):1159–72. https://doi.org/10.1007/s00228-023-03534-z PMID: 37420019

19. Begg M, Tarhuni M, N Fotso M, Gonzalez NA, Sanivarapu RR, Osman U, et al. Comparing the Safety and Efficacy of Proton Pump Inhibitors and Histamine-2 Receptor Antagonists in the Management of Patients With Peptic Ulcer Disease: A Systematic Review. Cureus. 2023;15(8):e44341. https://doi.org/10.7759/cureus.44341 PMID: 37779765

20. Lambert AA, Lam JO, Paik JJ, Ugarte-Gil C, Drummond MB, Crowell TA. Risk of community-acquired pneumonia with outpatient proton-pump inhibitor therapy: a systematic review and meta-analysis. PLoS One. 2015;10(6):e0128004. https://doi.org/10.1371/journal.pone.0128004 PMID: 26042842

21. Wu B, Li D, Xu T, Luo M, He Z, Li Y. Proton pump inhibitors associated acute kidney injury and chronic kidney disease: data mining of US FDA adverse event reporting system. Sci Rep. 2021;11(1):3690. https://doi.org/10.1038/s41598-021-83099-y PMID: 33574396

22. Laheij RJF, Sturkenboom MCJM, Hassing R-J, Dieleman J, Stricker BHC, Jansen JBMJ. Risk of community-acquired pneumonia and use of gastric acid-suppressive drugs. JAMA. 2004;292(16):1955–60. https://doi.org/10.1001/jama.292.16.1955 PMID: 15507580

23. Shah NH, LePendu P, Bauer-Mehren A, Ghebremariam YT, Iyer SV, Marcus J, et al. Proton Pump Inhibitor Usage and the Risk of Myocardial Infarction in the General Population. PLoS One. 2015;10(6):e0124653. https://doi.org/10.1371/journal.pone.0124653 PMID: 26061035

24. Yang Y-X, Lewis JD, Epstein S, Metz DC. Long-term proton pump inhibitor therapy and risk of hip fracture. JAMA. 2006;296(24):2947–53. https://doi.org/10.1001/jama.296.24.2947 PMID: 17190895

25. Janarthanan S, Ditah I, Adler DG, Ehrinpreis MN. Clostridium difficile-associated diarrhea and proton pump inhibitor therapy: a meta-analysis. Am J Gastroenterol. 2012;107(7):1001–10. https://doi.org/10.1038/ajg.2012.179 PMID: 22710578

26. Reich A, Maj J. Subacute cutaneous lupus erythematosus due to proton pump inhibitor intake: case report and literature review. Arch Med Sci. 2012;8(4):743–7. https://doi.org/10.5114/aoms.2012.30300 PMID: 23056090

27. Sandholdt LH, Laurinaviciene R, Bygum A. Proton pump inhibitor-induced subacute cutaneous lupus erythematosus. Br J Dermatol. 2014;170(2):342–51. https://doi.org/10.1111/bjd.12699 PMID: 24547721

28. Haenisch B, von Holt K, Wiese B, Prokein J, Lange C, Ernst A, et al. Risk of dementia in elderly patients with the use of proton pump inhibitors. Eur Arch Psychiatry Clin Neurosci. 2015;265(5):419–28. https://doi.org/10.1007/s00406-014-0554-0 PMID: 25341874

29. Gomm W, von Holt K, Thomé F, Broich K, Maier W, Fink A, et al. Association of Proton Pump Inhibitors With Risk of Dementia: A Pharmacoepidemiological Claims Data Analysis. JAMA Neurol. 2016;73(4):410–6. https://doi.org/10.1001/jamaneurol.2015.4791 PMID: 26882076

30. Jana K, Bandyopadhyay T, Ganguly B. Designed inhibitors with hetero linkers for gastric proton pump H+,K+-ATPase: Steered molecular dynamics and metadynamics studies. J Mol Graph Model. 2017;78:129–38. https://doi.org/10.1016/j.jmgm.2017.10.006 PMID: 29055186

31. Jana K, Chandar NB, Bandyopadhyay T, Ganguly B. Role of Noncovalent Interactions in Designing Inhibitors for H+,K+-ATPase: Combined QM and MD Based Investigations. ChemistrySelect. 2016;1(21):6847–54. https://doi.org/10.1002/slct.201601458

32. Scarpignato C, Hunt RH. Proton pump inhibitors: the beginning of the end or the end of the beginning?. Curr Opin Pharmacol. 2008;8(6):677–84. https://doi.org/10.1016/j.coph.2008.09.004 PMID: 18840545

33. Atanasov AG, Zotchev SB, Dirsch VM, International Natural Product Sciences Taskforce, Supuran CT. Natural products in drug discovery: advances and opportunities. Nat Rev Drug Discov. 2021;20(3):200–16. https://doi.org/10.1038/s41573-020-00114-z PMID: 33510482

34. Afrin MstF, Kabir E, Noyon MROK, Bhuiyan MMH, Shimu MSS, Alam MJ, et al. Spectrochemical, medicinal, and toxicological studies of ketoprofen and its newly designed analogs; quantum chemical, and drug discovery approach. Informatics in Medicine Unlocked. 2023;43:101399. https://doi.org/10.1016/j.imu.2023.101399

35. Chen J, Li W, Yao H, Xu J. Insights into drug discovery from natural products through structural modification. Fitoterapia. 2015;103:231–41. https://doi.org/10.1016/j.fitote.2015.04.012

36. Cheng Y, Ji Q, Zhu B, Zhang X, Gong H, Zhang Z. Manipulating fluorine induced bulky dipoles and their strong interaction to achieve high efficiency electric energy storage performance in polymer dielectrics. Chemical Engineering Journal. 2023;476:146738. https://doi.org/10.1016/j.cej.2023.146738

37. Senthilkumar K, Raman MS, Kolandaivel P. Effect of substitution of electron-donating and -withdrawing groups on the stability of flavin–diaminepyridine complexes—a density functional theory study. Journal of Molecular Structure: THEOCHEM. 2006;758(2–3):107–12. https://doi.org/10.1016/j.theochem.2005.10.009

38. Duvenhage MM, Visser HG, Ntwaeaborwa OM, Swart HC. The effect of electron donating and withdrawing groups on the morphology and optical properties of Alq3. Physica B: Condensed Matter. 2014;439:46–9. https://doi.org/10.1016/j.physb.2013.11.049

39. Uzzaman M, Chowdhury MK, Belal Hossen M. Thermochemical, Molecular docking and ADMET studies of Aspirin metabolites. Frontiers Drug Chemistry Clinical Res. 2019;2(3). https://doi.org/10.15761/fdccr.1000130

40. Santos L de A, Prandi IG, Ramalho TC. Could quantum mechanical properties be reflected on classical molecular dynamics? The case of halogenated organic compounds of biological interest. Front Chem. 2019;7:499693. https://doi.org/10.3389/fchem.2019.00848

41. Geerlings P, De Proft F, Langenaeker W. Conceptual density functional theory. Chem Rev. 2003;103(5):1793–873. https://doi.org/10.1021/cr990029p PMID: 12744694

42. Hasan MdB, Rahman MdJ, Das R, Akter T, Hosen MdS, Kona UMP, et al. Physicochemical, biological, and toxicological studies of pyridine and its derivatives: an in-silico approach. Discov Chem. 2025;2(1). https://doi.org/10.1007/s44371-025-00147-6

43. Petersilka M, Gossmann U, Gross E. Excitation energies from time-dependent density-functional theory. Phys Rev Lett. 1996;76(8):1212–5. https://doi.org/10.1103/PhysRevLett.76.1212 PMID: 10061664

44. Talukder MdEK, Atif MdF, Siddiquee NH, Rahman S, Rafi NI, Israt S, et al. Molecular docking, QSAR, and simulation analyses of EGFR-targeting phytochemicals in non-small cell lung cancer. Journal of Molecular Structure. 2025;1321:139924. https://doi.org/10.1016/j.molstruc.2024.139924

45. Meng X-Y, Zhang H-X, Mezei M, Cui M. Molecular docking: a powerful approach for structure-based drug discovery. Curr Comput Aided Drug Des. 2011;7(2):146–57. https://doi.org/10.2174/157340911795677602 PMID: 21534921

46. Mursal M, Ahmad M, Hussain S, Khan MF, Mursal M, Ahmad M, et al. Navigating the Computational Seas: A Comprehensive Overview of Molecular Docking Software in Drug Discovery. Unravelling Mol Docking - From Theory to Pract. 2024. https://doi.org/10.5772/INTECHOPEN.1004802

47. Jumper J, Evans R, Pritzel A, Green T, Figurnov M, Ronneberger O, et al. Highly accurate protein structure prediction with AlphaFold. Nature. 2021;596(7873):583–9. https://doi.org/10.1038/s41586-021-03819-2 PMID: 34265844

48. Guex N, Peitsch MC. SWISS-MODEL and the Swiss-PdbViewer: an environment for comparative protein modeling. Electrophoresis. 1997;18(15):2714–23. https://doi.org/10.1002/elps.1150181505 PMID: 9504803

49. Rana SM, Islam M, Saeed H, Rafique H, Majid M, Aqeel MT, et al. Synthesis, Computational Studies, Antioxidant and Anti-Inflammatory Bio-Evaluation of 2,5-Disubstituted-1,3,4-Oxadiazole Derivatives. Pharmaceuticals (Basel). 2023;16(7):1045. https://doi.org/10.3390/ph16071045 PMID: 37513956

50. Cheng F, Li W, Zhou Y, Shen J, Wu Z, Liu G, et al. admetSAR: a comprehensive source and free tool for assessment of chemical ADMET properties. J Chem Inf Model. 2012;52(11):3099–105. https://doi.org/10.1021/ci300367a PMID: 23092397

51. Dmitriev AV, Filimonov DA, Rudik AV, Pogodin PV, Karasev DA, Lagunin AA, et al. Drug-drug interaction prediction using PASS. SAR QSAR Environ Res. 2019;30(9):655–64. https://doi.org/10.1080/1062936X.2019.1653966 PMID: 31482727

52. Garbett NC, Chaires JB. Thermodynamic studies for drug design and screening. Expert Opin Drug Discov. 2012;7(4):299–314. https://doi.org/10.1517/17460441.2012.666235 PMID: 22458502

53. Kollman P. Free energy calculations: Applications to chemical and biochemical phenomena. Chem Rev. 1993;93(7):2395–417. https://doi.org/10.1021/cr00023a004

54. Uzzaman M, Hasan MdK, Mahmud S, Fatema K, Matin MM. Structure-based design of new diclofenac: Physicochemical, spectral, molecular docking, dynamics simulation and ADMET studies. Informatics in Medicine Unlocked. 2021;25:100677. https://doi.org/10.1016/j.imu.2021.100677

55. Uddin MN, Uzzaman M, Das S, Al-Amin Md, Haque Mijan MdN. Stress degradation, structural optimization, molecular docking, ADMET analysis of tiemonium methylsulphate and its degradation products. Journal of Taibah University for Science. 2020;14(1):1134–46. https://doi.org/10.1080/16583655.2020.1805186

56. Azam F, Alabdullah NH, Ehmedat HM, Abulifa AR, Taban I, Upadhyayula S. NSAIDs as potential treatment option for preventing amyloid β toxicity in Alzheimer's disease: an investigation by docking, molecular dynamics, and DFT studies. J Biomol Struct Dyn. 2018;36(8):2099–117. https://doi.org/10.1080/07391102.2017.1338164 PMID: 28571516

57. Ramalingam S, Karabacak M, Periandy S, Puviarasan N, Tanuja D. Spectroscopic (infrared, Raman, UV and NMR) analysis, Gaussian hybrid computational investigation (MEP maps/HOMO and LUMO) on cyclohexanone oxime. Spectrochim Acta A Mol Biomol Spectrosc. 2012;96:207–20. https://doi.org/10.1016/j.saa.2012.03.090 PMID: 22683556

58. Uzzaman M, Mahmud T. Structural modification of aspirin to design a new potential cyclooxygenase (COX-2) inhibitors. In Silico Pharmacol. 2020;8(1):1. https://doi.org/10.1007/s40203-020-0053-0 PMID: 32181121

59. Politzer P, Murray JS. Molecular Electrostatic Potentials. ChemInform. 2004;35(27). https://doi.org/10.1002/chin.200427290

60. Güntepe F, Çinarli M, Kazak C, Bati H. Spectroscopic and Quantum Chemical Studies of (Z)-N′-(3-(hidroksiimino)butan-2-ylidene)-4-metilbenzensulfonohidrazide Ligand. Molecular Crystals and Liquid Crystals. 2015;616(1):213–25. https://doi.org/10.1080/15421406.2014.991135

61. Murray JS, Politzer P. Molecular electrostatic potentials and noncovalent interactions. WIREs Comput Mol Sci. 2017;7(6). https://doi.org/10.1002/wcms.1326

62. Mohan N, Suresh CH. A molecular electrostatic potential analysis of hydrogen, halogen, and dihydrogen bonds. J Phys Chem A. 2014;118(9):1697–705. https://doi.org/10.1021/jp4115699 PMID: 24506527

63. Kireev DB, Fetisov VI, Zefirov NS. Approximate molecular electrostatic potential computations: applications to quantitative structure-activity relationships. Journal of Molecular Structure: THEOCHEM. 1994;304(2):143–50. https://doi.org/10.1016/s0166-1280(96)80006-6

64. Ahluwalia VK. Ultraviolet Spectroscopy. Instrumental Methods of Chemical Analysis. Springer Nature Switzerland; 2023. 233–69. https://doi.org/10.1007/978-3-031-38355-7_24

65. Gill DM, R Povinelli AP, Zazeri G, Shamir SA, Mahmoud AM, Wilkinson FL, et al. The modulatory role of sulfated and non-sulfated small molecule heparan sulfate-glycomimetics in endothelial dysfunction: absolute structural clarification, molecular docking and simulated dynamics, SAR analyses and ADMET studies. RSC Med Chem. 2021;12(5):779–90. https://doi.org/10.1039/d0md00366b PMID: 34124676

66. Matin MM, Hasan MdS, Uzzaman M, Bhuiyan MdMH, Kibria SM, Hossain MdE, et al. Synthesis, spectroscopic characterization, molecular docking, and ADMET studies of mannopyranoside esters as antimicrobial agents. Journal of Molecular Structure. 2020;1222:128821. https://doi.org/10.1016/j.molstruc.2020.128821

67. Sun H, Chow EC, Liu S, Du Y, Pang KS. The Caco-2 cell monolayer: usefulness and limitations. Expert Opin Drug Metab Toxicol. 2008;4(4):395–411. https://doi.org/10.1517/17425255.4.4.395 PMID: 18433344

68. Finch A, Pillans P. P-glycoprotein and its role in drug-drug interactions. Aust Prescr. 2014;37(4):137–9. https://doi.org/10.18773/austprescr.2014.050

69. Amin ML. P-glycoprotein Inhibition for Optimal Drug Delivery. Drug Target Insights. 2013;7:27–34. https://doi.org/10.4137/DTI.S12519 PMID: 24023511

70. Matin MM, Bhuiyan MMH, Kabir E, Sanaullah AFM, Rahman MA, Hossain ME, et al. Synthesis, characterization, ADMET, PASS predication, and antimicrobial study of 6-O-lauroyl mannopyranosides. Journal of Molecular Structure. 2019;1195:189–97. https://doi.org/10.1016/j.molstruc.2019.05.102

71. Guan L, Yang H, Cai Y, Sun L, Di P, Li W, et al. ADMET-score - a comprehensive scoring function for evaluation of chemical drug-likeness. Medchemcomm. 2019;10(1):148–57. https://doi.org/10.1039/c8md00472b PMID: 30774861

72. Anzali S, Barnickel G, Cezanne B, Krug M, Filimonov D, Poroikov V. Discriminating between drugs and nondrugs by prediction of activity spectra for substances (PASS). J Med Chem. 2001;44(15):2432–7. https://doi.org/10.1021/jm0010670 PMID: 11448225

73. Lagunin A, Stepanchikova A, Filimonov D, Poroikov V. PASS: prediction of activity spectra for biologically active substances. Bioinformatics. 2000;16(8):747–8. https://doi.org/10.1093/bioinformatics/16.8.747 PMID: 11099264

74. Akash S, Bayıl I, Rahman MA, Mukerjee N, Maitra S, Islam MR, et al. Target specific inhibition of West Nile virus envelope glycoprotein and methyltransferase using phytocompounds: an in silico strategy leveraging molecular docking and dynamics simulation. Front Microbiol. 2023;14:1189786. https://doi.org/10.3389/fmicb.2023.1189786 PMID: 37455711

75. Siddiquee NH, Malek S, Tanni AA, Mitu IJ, Arpa SH, Hasan MR, et al. Unveiling the antiviral activity of 2′,3,5,7-Tetrahydroxyflavanone as potential inhibitor of chikungunya virus envelope glycoprotein. Informatics in Medicine Unlocked. 2024;47:101486. https://doi.org/10.1016/j.imu.2024.101486

76. Ahammad F, Alam R, Mahmud R, Akhter S, Talukder EK, Tonmoy AM, et al. Pharmacoinformatics and molecular dynamics simulation-based phytochemical screening of neem plant (Azadiractha indica) against human cancer by targeting MCM7 protein. Brief Bioinform. 2021;22(5):bbab098. https://doi.org/10.1093/bib/bbab098 PMID: 33834183

77. Siddiquee NH, Hossain MI, Talukder MEK, Nirob SAA, Shourav M, Jahan I, et al. In-silico identification of novel natural drug leads against the Ebola virus VP40 protein: A promising approach for developing new antiviral therapeutics. Informatics in Medicine Unlocked. 2024;45:101458. https://doi.org/10.1016/j.imu.2024.101458

78. Ghahremanian S, Rashidi MM, Raeisi K, Toghraie D. Molecular dynamics simulation approach for discovering potential inhibitors against SARS-CoV-2: A structural review. J Mol Liq. 2022;354:118901. https://doi.org/10.1016/j.molliq.2022.118901 PMID: 35309259

79. Kolybalov DS, Kadtsyn ED, Arkhipov SG. Computer Aided Structure-Based Drug Design of Novel SARS-CoV-2 Main Protease Inhibitors: Molecular Docking and Molecular Dynamics Study. Computation. 2024;12(1):18. https://doi.org/10.3390/computation12010018

80. Eskandarzadeh M, Kordestani-Moghadam P, Pourmand S, Khalili Fard J, Almassian B, Gharaghani S. Inhibition of GSK_3β by Iridoid Glycosides of Snowberry (Symphoricarpos albus) Effective in the Treatment of Alzheimer's Disease Using Computational Drug Design Methods. Front Chem. 2021;9:709932. https://doi.org/10.3389/fchem.2021.709932 PMID: 34692636

81. Islam R, Parves MR, Paul AS, Uddin N, Rahman MS, Mamun AA, et al. A molecular modeling approach to identify effective antiviral phytochemicals against the main protease of SARS-CoV-2. J Biomol Struct Dyn. 2021;39(9):3213–24. https://doi.org/10.1080/07391102.2020.1761883 PMID: 32340562

82. J. R. Yunta M. It Is Important to Compute Intramolecular Hydrogen Bonding in Drug Design?. AJMO. 2017;5(1):24–57. https://doi.org/10.12691/ajmo-5-1-3

83. Panigrahi SK. Strong and weak hydrogen bonds in protein-ligand complexes of kinases: a comparative study. Amino Acids. 2008;34(4):617–33. https://doi.org/10.1007/s00726-007-0015-4 PMID: 18180869

84. Opo FADM, Rahman MM, Ahammad F, Ahmed I, Bhuiyan MA, Asiri AM. Structure based pharmacophore modeling, virtual screening, molecular docking and ADMET approaches for identification of natural anti-cancer agents targeting XIAP protein. Sci Rep. 2021;11(1):4049. https://doi.org/10.1038/s41598-021-83626-x PMID: 33603068

85. Bharadwaj S, Dubey A, Yadava U, Mishra SK, Kang SG, Dwivedi VD. Exploration of natural compounds with anti-SARS-CoV-2 activity via inhibition of SARS-CoV-2 Mpro. Brief Bioinform. 2021;22(2):1361–77. https://doi.org/10.1093/bib/bbaa382 PMID: 33406222